I&EC research
Industrial & Engineering Chemistry Research

pubs.acs.org/IECR
Article

Supercritical Water Gasification of Ethanol as Biomass Model Compound in Tandem with Steam Reforming: Kinetic Modeling of the Reforming Step and Techno-Economic Analysis of the Integrated Concept

Athanasios A. Vadarlis,* Bruno Lacerda de Oliveira Campos, Angeliki A. Lemonidou, Nikolaos Boukis, and Jörg Sauer

Cite This: *Ind. Eng. Chem. Res.* 2024, 63, 16683−16700

Read Online

ACCESS | Metrics & More | Article Recommendations | Supporting Information

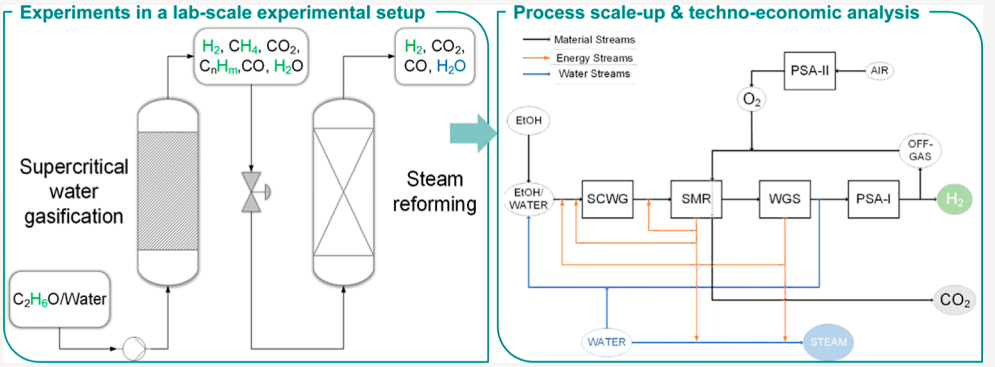

ABSTRACT: The integration of "biomass gasification with supercritical water ", "steam reforming of hydrocarbons", and "water−gas shift reaction" is a promising process concept for the conversion of moist biomass to "green hydrogen". This process concept was investigated in this work, considering ethanol as a biomass model compound. The gasification of ethanol with supercritical water can be accurately simulated, allowing a very good prediction of the gaseous product that will undergo steam reforming. A multidisciplinary study is presented, in which a comprehensive kinetic model for steam reforming of the gasification product gas was developed and validated with experimental data and then employed in a simulation of the whole process chain. Finally, a techno-economic and sensitivity analysis was applied. In the kinetic model, the high steam content overshadowed the influence of other substances in the sites balance on the catalyst surface, except for methane. After investigating the effect of ethanol concentration and feed flow rate, and considering the technical constraints imposed by the high organic matter content and the availability of actual waste biomass, the optimal values of the ethanol concentration and feed flow rate were 50 t h^{-1} and 15 wt % ethanol, reaching a hydrogen break-even price of 6.8 \$ $kg_{H_2}^{-1}$. The sensitivity analysis identified the ethanol price as the primary cost driver. Exploring waste biomass feedstocks, such as sewage sludge, demonstrated potential break-even prices as low as 0−1.8 \$ $kg_{H_2}^{-1}$, which can compete with conventional technologies.

INTRODUCTION

The energy transition toward zero carbon emissions is going to rely heavily on hydrogen production.[1] A promising technology for sustainable hydrogen production is the gasification of waste biomass resources. In particular, the supercritical water gasification (SCWG) is an ideal process for waste biomass with high water content that cannot be processed effectively with conventional gasification techniques due to required predrying.[2]

Under supercritical conditions (T > 374 °C, p > 221 bar), the water facilitates the hydrolysis of the biomass long chain organic molecules, turning them to their monomers.[3] The latter react then with water to generate H_2, CO, and CO_2[4] (eqs 1 and 2). Carbon monoxide reacts with H_2 to form CH_4 (via eq 3) and with steam to produce CO_2 (eq 4)[5]

$$C_xH_yO_z + (x - z)H_2O \rightarrow xCO + \left(x - z + \frac{y}{2}\right)H_2 \quad (1)$$

Received: April 19, 2024
Revised: August 26, 2024
Accepted: August 26, 2024
Published: September 18, 2024

https://doi.org/10.1021/acs.iecr.4c01486
Ind. Eng. Chem. Res. 2024, 63, 16683−16700

$$C_xH_yO_z + (2x - z)H_2O \rightarrow xCO_2 + \left(2x - z + \frac{y}{2}\right)H_2 \quad (2)$$

$$CO + 3H_2 \rightleftarrows CH_4 + H_2O \qquad \Delta H^0 = -206.1\ \text{kJ·mol}^{-1} \quad (3)$$

$$CO + H_2O \rightleftarrows CO_2 + H_2 \qquad \Delta H^0 = -41.2\ \text{kJ·mol}^{-1} \quad (4)$$

Additional chemical reactions occur, which generate coke, tars, and heavier hydrocarbons (mainly ethane),[6] all depending on the conditions of SCWG, the presence of catalysts, and the biomass structure and composition.[7−9] The SCWG of organics started gaining notable interest in the 1980s. For instance, Model investigated the gasification of glucose using both subcritical and supercritical water.[10] The key finding was that no char formed in the supercritical state, unlike in the subcritical state, suggesting that supercritical water acts as an efficient solvent, keeping organic compounds uniformly dispersed. Since then, the field has gained significant development and progress, addressing various challenges such as transition to real waste biomass, char formation, poor gasification yields, corrosion, and plugging issues.[3] However, a research gap remains in optimizing the SCWG process to enhance hydrogen production. A portion of the produced hydrogen remains bound to the coproduced hydrocarbons, which impacts the efficiency of hydrogen recovery. A recent review from our group of experimental research on catalytic SCWG of organics found that, in most cases, a significant amount of the hydrogen produced (around 30%) was bound to the hydrocarbons, mainly methane. In comparison, in cases where less than 5% of the hydrogen produced was trapped in the hydrocarbons, the feed was quite dilute (≤5 wt %), and the operating temperature exceeded 700 °C.[11]

To increase the H_2 yield, a subsequent steam or dry reforming process of the SCWG product gas is required.[12,13] Steam reforming of natural gas or steam methane reforming (SMR) is the most widely used industrial technology for hydrogen production.[14] In this process, steam reacts with CH_4 (eqs 5 and 6) under high temperature (700−1000 °C), in the pressure range 20−30 bar and at steam to CH_4 (H_2O/CH_4) ratios of 2.5−3,[15−17] producing H_2, CO and CO_2.

$$CH_4 + H_2O \rightleftarrows CO + 3H_2 \qquad \Delta H^0 = 206.1\ \text{kJ·mol}^{-1} \quad (5)$$

$$CH_4 + 2H_2O \rightleftarrows CO_2 + 4H_2 \qquad \Delta H^0 = 164.9\ \text{kJ·mol}^{-1} \quad (6)$$

The produced CO reacts with the remaining steam to result in CO_2 and H_2, via the water−gas shift (WGS) reaction (eq 4). Should the feed to the steam reformer consist of heavier hydrocarbons, they also react with steam according to eq 7[18,19]

$$C_nH_m + nH_2O \rightarrow nCO + \left(\frac{m}{2} + n\right)H_2 \quad (7)$$

In parallel carbon formation reactions can also take place.[20] This process is conducted in the presence of a Ni-based catalyst.[21,22]

Several studies have implemented the combination of biomass SCWG and subsequent steam/dry reforming with simulations in Aspen Plus. Hantoko et al.[23] simulated a process for the SCWG of sewage sludge and the subsequent SMR of the product gas at the same pressure of the SCWG reactor, concluding that the reformer's implementation significantly increased the systems energetic efficiency and the H_2 yield. Ruya et al.[12] assessed the incorporation of a steam reformer in an autothermal process of SCWG of empty fruit bunch and palm oil mill effluent. They reported that the implementation of the steam reformer at the lowest biomass concentration (15 wt % of empty fruit bunch) decreased the net H_2 yield because the product gas only covered the energy demands of the process. In contrast, at high biomass concentrations (25 wt %), the reformer's implementation increased the net H_2 yield up to 98%. Campanario and Gutiérrez Ortiz designed and simulated a process for the SCWG of the bio-oil aqueous phase coupled with dry reforming of the produced syngas and purification with a pressure swing adsorption (PSA) unit. The authors also assessed this process techno-economically.[24] Kumar et al.[25] proposed a process for the SCWG of microalgae, implementing a mineral separator step upstream of the SCWG and an SMR reactor followed by high and low temperature WGS reactors, downstream of the SCWG reactor and after water separation. They reported that for a plant capacity of 2000 t d^{-1}, a total capital investment of 277.8 M $ (in 2019) was required, with a respective hydrogen price of 4.59 ± 0.1 $ kg^{-1}.

There is a lack of experimental work covering steam reforming of the product gas from SCWG for increased hydrogen production. Brito et al.[6] performed steam reforming of the gas produced from gasification of lignin with oxygen and steam. Their experiments were conducted at 500−800 °C, 1 atm, a ratio of steam to carbon present in CH_4 and C_2H_6 in the feed equal to 3, and space velocity 0.5 Nl min^{-1} g_{cat}^{-1}. While a significant amount of methane was observed at 500 °C, due to an unfavorable chemical equilibrium at lower temperatures, full CH_4 conversion was observed at 800 °C. Additionally, they demonstrated that complete ethane conversion was reached for $T \geq 750$ °C. Their thermodynamic analysis showed that to optimize hydrogen yield while mitigating coke formation, a minimum temperature of 700 °C and a steam-to-carbon (S/C) ratio between 2 and 3 are required. At lower temperatures and/or lower S/C ratios, coke formation is more likely. To inhibit coke formation at very low S/C ratios, in the absence of water, or when higher hydrocarbons are present in the feed, the pioneering work of Subramaniam et al.[26−28] suggests that under dense supercritical conditions, coke solubility in the reaction mixture is enhanced. This prevents coke deposition and buildup inside the pores, thereby avoiding pore plugging.

The analysis of Brito et al.[6] focused on the subsequent steam reforming of the gas produced from biomass gasification under ambient pressures, and not specifically of product gases resulting from SCWG. To address this gap of experimental work a lab-scale setup combining SCWG with direct subsequent steam reforming was conceptualized and investigated. This concept was also applied for a patent.[29] The experimental work has been reported in a recent study by our group, where the first two reactors from the conceptualized process—the SCWG reactor and the steam reformer—were operated.[30] In that study, ethanol was used as a model compound for biomass. It was demonstrated that the total hydrogen yield based on the EtOH in the feed increased significantly, from 27.4% with only the SCWG reactor (gasification of 8 wt % EtOH, at 250 bar, 600 °C, and 1.5 min residence time), to 98% with the SMR reactor's integration, at 600 °C, 1 atm and a gas hourly space velocity (GHSV) of around 14,850 h^{-1}. The excess steam left over from gasification entered the second reactor together with the product gas, promoted the SMR reaction even at low

https://doi.org/10.1021/acs.iecr.4c01486
Ind. Eng. Chem. Res. 2024, 63, 16683−16700

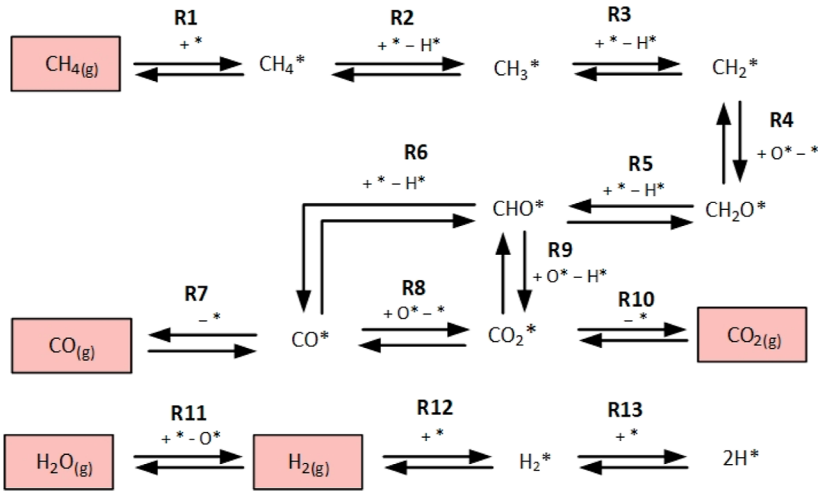

Figure 1. Reaction mechanism of SMR and WGS from Xu and Froment.[41] The asterisk symbol (*) denotes a free active site on the catalyst surface. The reaction numeration was modified. Reproduced with permission from Xu and Froment.[41] Copyright 2024 John Wiley and Sons.

temperatures (450−550 °C), inhibited the formation of carbon deposits on the catalyst, but enhanced the sintering of the active metal. After successful experimental investigation it is of great interest to study the economics of the process. In the present study a techno-economic analysis was conducted based on the experimental results produced previously.

The development of alternative processes to replace conventional technologies for processing fossil fuels, requires thorough economic analysis. A techno-economic analysis can assess the profitability of the proposed process, identify strategies for cost minimization, and ultimately compare its competitiveness with other conventional processes. Within this context a new kinetic model was developed to describe the kinetics of methane and ethane reforming based on the experiments carried out in the previous work of the group,[30] and is the first model to describe this reaction at such high steam content ($13 \leq H_2O/CH_4 \leq 46$), to the best of our knowledge. The model was applied in Aspen HYSYS V14 to scale up the experimentally developed process, incorporating technologies like oxyfuel combustion to reduce its carbon footprint on an industrial scale. Finally, an economic analysis was carried out to determine the cost of such a chemical plant, considering as important parameters the organic matter concentration in the feed and the plant capacity in order to minimize the cost of hydrogen production. A follow-up sensitivity analysis helped to identify the most significant contributors to the cost of hydrogen produced. As a benchmark for comparing hydrogen production costs, recent studies suggest that by 2030, the cost of hydrogen produced through electrolysis in the EU will range between €3 and €5 per kilogram.[31−34]

It should be noted that the process used EtOH as a biomass model compound because this substance was also used for the laboratory experiments in the previous work of the group. Ethanol can be used as a biomass model compound to model the complete gasification with supercritical water of sewage sludge and microalgae. Ethanol is composed of 52.17 wt % C, 13.04 wt % H, and 34.78 wt % O. Although the composition of microalgae and sewage sludge may vary, there have been several studies in the literature with compositions similar to EtOH with respect to the three components mentioned.[35−40] It should be mentioned, however, that the amount of ash in real biomasses should not be taken into account for the comparison. Furthermore, this work aims to formulate a base case that is not affected by obstacles like coke formation, salt deposition and eventually incomplete gasification and plugging as it might be the case when processing waste biomasses.[8] After successful process assessment with EtOH further investigation and development is required for processing waste biomasses.

MATERIALS AND METHODS

Experimental Layout and Procedure. A comprehensive overview of the experimental methodology, setup details, and additional information was previously presented in the aforementioned work.[30] Still, a shorter description is provided here with specific reference to the information most relevant to the present work.

The experimental setup includes a feeding system with an EtOH/water solution, an HPLC pump, two tubular reactors of 8 mm i.d., and two back-pressure regulators, one installed at the outlet of the first reactor (SCWG) and the other at the outlet of the second reactor (reforming).

The reforming reactor is connected in series with the first reactor, and it contains a fixed catalytic bed with a commercial Ni-based catalyst (ReforMax 210 LDP, purchased from C&CS Catalysts and Chemicals Specialties GmbH). Its nominal content of NiO is 18 wt % and it is supported on a $CaK_2Al_{22}O_{34}$ support. It was delivered in the form of 10-hole ring-shaped pellets, which were crushed and sieved into particles with a diameter in the range 250−500 μm. Its apparent density is 0.915 g cm^{-3}. The BET surface area of the fresh and reduced catalyst was measured to be equal to 3.8 and 14.6 m^2 g_{cat}^{-1}, respectively.[30]

The SCWG of 8 wt % EtOH was performed at 600 °C and 250 bar.[30] The residence time in the SCWG reactor was 1.5 min (calculated at experimental conditions, i.e., 600 °C and 250 bar). The investigated operating parameters in SMR reactor were the temperature (450−700 °C), the pressure (1−40 bar), and the GHSV (14,852−74,163 h^{-1}). The latter parameter was studied by adjusting the amount of catalyst in the SMR reactor. In addition, some experiments were performed that are not part of the previous publication and involve different EtOH concentrations, namely 5, 11, and 13 wt %. In the latter experiments, the amount of catalyst in the second reactor was adjusted so that the ratio of the flow of the SCWG dry product gas to the volume of the catalytic bed of the SMR reactor (i.e., $\frac{\dot{Q}_{SCWG,dry}}{V_{SMR,cat.bed}}$) to be 6 ×

https://doi.org/10.1021/acs.iecr.4c01486
Ind. Eng. Chem. Res. 2024, 63, 16683−16700

10^{-3} h^{-1}. All the experimental data are listed in Tables S1 and S2 (Chapter S1) in the Supporting Information.

Kinetic Model of the SMR Reactor. *Kinetic Model of Xu and Froment for SMR.* Xu and Froment[41] developed a model for SMR and the WGS reaction. They considered three global reactions: SMR with CO formation (eq 5), SMR with CO_2 formation (eq 6), and the WGS (eq 4). The reaction mechanism from Xu and Froment is provided in Figure 1, while a table with the list of elementary reactions is presented in the Supporting Information (see Table S3).

According to Xu and Froment, R6 is the rate-determining step (RDS) of SMR to CO, R9 is the RDS of SMR to CO_2, and R8 is the RDS of WGS. After defining the reaction mechanism and the rate-determining steps, the reaction rates (r_i, in mol·kg_{cat}^{-1} s^{-1}) for R6 (eq 8), R9 (eq 9), and R8 (eq 10) were derived

$$\text{SMR to CO, RDS is R6: } r_1 = k_1 \cdot \theta_*^2 \cdot \left(\frac{p_{CH_4} \cdot p_{H_2O}}{p_{H_2}^{2.5}} - \frac{p_{H_2}^{0.5} \cdot p_{CO}}{K_{P,1}^0} \right) \tag{8}$$

$$\text{SMR to } CO_2\text{, RDS is R9: } r_2 = k_2 \cdot \theta_*^2 \cdot \left(\frac{p_{CH_4} \cdot p_{H_2O}^2}{p_{H_2}^{3.5}} - \frac{p_{H_2}^{0.5} \cdot p_{CO_2}}{K_{P,2}^0} \right) \tag{9}$$

$$\text{WGS, RDS is R8: } r_3 = k_3 \cdot \theta_*^2 \cdot \left(\frac{p_{CO} \cdot p_{H_2O}}{p_{H_2}} - \frac{p_{CO_2}}{K_{P,3}^0} \right) \tag{10}$$

where k_i is the constant of reaction i (k_1 and k_2 in mol·kg_{cat}^{-1} s^{-1} $bar^{0.5}$, k_3 in mol·kg_{cat}^{-1} s^{-1} bar^{-1}), p_j is the partial pressure of component j (bar), $K_{P,i}^0$ is the equilibrium constant of reaction i ($K_{P,1}^0$ and $K_{P,2}^0$ in $bar^{1.5}$, $K_{P,3}^0$ in bar), and θ_* is the fraction of free active sites on the catalyst surface (in the original work, it was defined as 1/DEN), which was calculated by a balance equation (eq 11)

$$\theta_* = (1 + K_{CO} \cdot p_{CO} + K_{CH_4} \cdot p_{CH_4} + K_{H_2} \cdot p_{H_2} + K_{H_2O} \cdot p_{H_2O} \cdot p_{H_2}^{-1})^{-1} \tag{11}$$

where, K_j is the adsorption constant related to component j (K_{CO}, K_{CH_4}, and K_{H_2} are in bar^{-1}, while K_{H_2O} is unitless). Xu and Froment stated that CO_2 adsorption was not significant and, therefore, not considered in the balance equation.

The reaction constants (k_i) and the adsorption constants (K_j) were described via the Arrhenius equation (given in eqs 12 and 13, in the original work, the terms A_i and $A_{ad,i}$ in the Arrhenius equation were outside the exponential function).

$$k_i = \exp\left[A_i - \frac{E_{A_i}}{R} \cdot \left(\frac{1}{T} - \frac{1}{T_{ref}} \right) \right] \tag{12}$$

$$K_j = \exp\left[A_{ad,i} - \frac{\Delta H_j}{R} \cdot \left(\frac{1}{T} - \frac{1}{T_{ref}} \right) \right] \tag{13}$$

where A_i and $A_{ad,i}$ are pre-exponential factors, $E_{A,i}$ is the activation energy, T_{ref} is the reference temperature of the kinetic model (in this work, T_{ref} = 873.15 K), and ΔH_j is the enthalpy variation of the adsorption.

In total, the model of the original work has 14 parameters to be fitted to the experiments, i.e., A_1, A_2, A_3, E_{A_1}, E_{A_2}, E_{A_3}, $A_{ad,CO}$, A_{ad,CH_4}, A_{ad,H_2}, A_{ad,H_2O}, ΔH_{CO}, ΔH_{CH_4}, ΔH_{H_2}, ΔH_{H_2O}.

Kinetic Model of the Present Work for SMR and SER. In general, mathematical models should be as simple as possible and as complex as necessary. Furthermore, the number of fitted parameters should also be minimized to avoid highly correlated and statistically insignificant parameters. Therefore, this paper presents a modified version of Xu and Froment's model, with a focus on a steam-rich operating window, thereby reducing model complexity and the number of parameters.

The WGS is reported to be rapid under reforming conditions;[42−44] therefore, its actual kinetic parameters are difficult to estimate.[43] If the WGS is considered rapid under typical SMR conditions, it should be even faster when steam is in large excess. Because of that, we assumed this reaction to be quasi-equilibrated. Mathematically, this was done by assuming a high value for the WGS reaction constant, avoiding parameter fitting. The values of A_3 = 5 and E_{A_3} = 0 kJ mol^{-1} were found to be high enough to guarantee quasi-equilibrium conditions, while not too high to create numerical instability. A similar procedure was performed in the literature for a SMR kinetic model at typical operating conditions.[43]

The SMR system is described by three global reactions (eqs 4−6). However, because each reaction is a linear combination of the other two, two reactions might be enough to represent the system, allowing a reduction in the model's complexity. Since the WGS is much faster than SMR, it should not be excluded. Therefore, two possibilities were considered in this work: (i) WGS and SMR to CO (eqs 4 and 5), (ii) WGS and SMR to CO_2 (eqs 4 and 6).

The elementary step R5 was also tested as RDS for SMR. Since this step belongs to both SMR to CO and SMR to CO_2, and the WGS is considered rapid, the same results would be achieved if considering either CO or CO_2 as the product. Therefore, this approach was only tested for SMR to CO, and the reaction rate was derived. A detailed mathematical derivation of eq 14 is provided in the Supporting Information (see Chapter S2).

$$\text{SMR to CO, RDS is R5: } r_1 = k_1 \cdot \theta_*^2 \cdot \left(\frac{p_{CH_4} \cdot p_{H_2O}}{p_{H_2}^2} - \frac{p_{H_2} \cdot p_{CO}}{K_{P,1}^0} \right) \tag{14}$$

It was not possible to get statistically significant parameters for K_{CO} and K_{H_2}. In the work of Xu and Froment,[41] K_{CO} and K_{H_2} could only be defined by performing reverse WGS + methanation experiments. Such experiments are out of scope in the present study, and only the adsorption constants of the reactants (K_{CH_4} and K_{H_2O}) were considered. Furthermore, because the present work focuses on much higher steam content ($13 \le H_2O/CH_4 \le 46$) in comparison with the typically studied range in the literature ($0.25 \le H_2O/CH_4 \le 6$),[45] it is likely that the adsorption constants of the products do not play as a significant role as in typical conditions. Therefore, eq 11 was simplified (eq 15).

$$\theta_* = (1 + K_{CH_4} \cdot p_{CH_4} + K_{H_2O} \cdot p_{H_2O} \cdot p_{H_2}^{-1})^{-1} \tag{15}$$

https://doi.org/10.1021/acs.iecr.4c01486
Ind. Eng. Chem. Res. 2024, 63, 16683−16700

The temperature dependent parameters of the adsorption constants (ΔH_j) were not statistically significant, so that K_{CH_4} and K_{H_2O} were estimated as single parameters.

Finally, low amounts of ethane are contained in the feed streams, and steam ethane reforming (SER) also takes place on the catalyst surface. At reforming conditions, the reverse reaction is negligible: $K^0_{P,SER}$ (873 K) = 5600, $K^0_{P,SER}$ (973 K) = 1,140,000.[46] Thus, irreversible SER was considered (eq 16).

$$C_2H_6 + 2\cdot H_2O \rightarrow 2\cdot CO + 5\cdot H_2 \qquad \Delta H^0 = 346.3\ \text{kJ}\cdot\text{mol}^{-1} \tag{16}$$

A literature search was made regarding SER, but no kinetic models were found. Furthermore, the ethane concentration in this study is extremely low compared to steam (H_2O/C_2H_6 > 450), thus it is expected that the steam apparent order is either zero or even negative. Therefore, the simplest assumption was made, i.e., the reaction rate of SER is first order in relation to ethane and independent of steam partial pressure (eq 17)

$$\text{SER: } r_4 = k_4\cdot p_{C_2H_6} \tag{17}$$

where r_4 is in mol·kg_{cat}^{-1} s^{-1}. To summarize, three kinetic models were developed and compared. While the same rates for WGS (eq 10), SER (eq 17) and the same fraction of active sites (eq 15) were considered, the models differ concerning SMR. That is:

- model M1—SMR to CO, R6 is the RDS (eq 8)
- model M2—SMR to CO_2, R9 is the RDS (eq 9)
- model M3—SMR to CO, R5 is the RDS (eq 14)

The equilibrium constants ($K^0_{P,1-3}$) were taken from the database of Goos et al.,[46] which contains 7-parameter temperature-dependent functions. A parametrization to 3-parameter functions was made in the temperature interval of 700−1100 K, and an average relative error below 0.1% was obtained. The resulting functions are provided as follows (eqs 18−20)

$$K^0_{P,1} = T^{1.878}\cdot\exp(15.58 - 25256\cdot T^{-1}) \tag{18}$$

$$K^0_{P,2} = T^{3.118}\cdot\exp(1.96 - 19,836\cdot T^{-1}) \tag{19}$$

$$K^0_{P,3} = T^{1.259}\cdot\exp(-13.77 + 5437\cdot T^{-1}) \tag{20}$$

Modeling of the SMR Reactor. To simulate the operating conditions of the SMR laboratory experiments, the following assumptions were made: (i) plug flow reactor (PFR), (ii) isobaric conditions, (iii) isothermal conditions, and (iv) variations only along the reactor length (1D approach). Component and total molar balance along the reactor length were then derived (eqs 21 and 22).

$$\frac{d\dot{n}}{dz} = \frac{m_{Cat}}{L}\cdot\sum_{j=1}^{N_C}\sum_{i=1}^{N_R}(\nu_{ji}\cdot r_i) \tag{21}$$

$$\frac{dy_j}{dz} = \frac{1}{\dot{n}}\cdot\left\{\frac{m_{Cat}}{L}\cdot\sum_{i=1}^{N_R}(\nu_{ji}\cdot r_i) - y_j\cdot\frac{d\dot{n}}{dz}\right\} \tag{22}$$

Here, $\dot{n}$ is the total mole flow (mol·s^{-1}), m_{Cat} is the total catalyst mass (kg), L is the catalytic bed length (m), N_R is the number of reactions, N_C is the number of components, ν_{ji} is the stoichiometric coefficient of component j in reaction i, and y_i is the mole fraction of component j.

The differential equations were implemented in Matlab and solved with the built-in function *ode45*, with absolute and relative tolerances set to 10^{-6}.

Estimation of the Kinetic Parameters. Since a high value for the WGS constant was assumed ($A_3 = 5$ and $E_{A_3} = 0$), each model has a maximum of six parameters to be fitted to the experiments:

- For M1 and M3: A_1, A_4, E_{A_1}, E_{A_4}, K_{CH_4}, and K_{H_2O}
- For M2: A_2, A_4, E_{A_2}, E_{A_4}, K_{CH_4}, and K_{H_2O}

An optimization problem was solved to estimate the kinetic parameters. Its objective function was the minimization of the normalized squared deviations between the experimental data and the simulations (f_{min}), i.e., the chi-square method (χ^2). Since the WGS is considered fast, and only the SMR and SER kinetic parameters need to be estimated, methane and ethane conversion values are sufficient to describe the system. Thus, the following objective function was applied (eq 23)

$$\chi^2 = f_{min}\sum_{i=1}^{N_{TP}}\left[\left(\frac{X_{CH_4,i} - \hat{X}_{CH_4,i}}{X_{CH_4,i}}\right)^2 + \left(\frac{X_{C_2H_6,i} - \hat{X}_{C_2H_6,i}}{X_{C_2H_6,i}}\right)^2\right] \tag{23}$$

where N_{TP} is the number of training points, and X_j and $\hat{X}_j$ are the measured and simulated values of component j conversion, respectively. The inverse of the squared experimental values was used as weights to avoid giving too much weight to high conversion points and too less weight to low conversion points.

The optimization problem was solved in Matlab with the built-in function *fminsearch*, with the step tolerance set to 5×10^{-3} and the function tolerance set to 10^{-3}.

To assess the model accuracy outside the training region, the 5-fold cross-validation method was applied. It consists of dividing the database into five groups of equal size and solving the optimization problem five times, each time leaving a different group out for validation only. Finally, χ^2 was calculated for all points for each set of optimized parameters (eq 24).

$$\chi^2_{all} = \sum_{i=1}^{N_P}\left[\left(\frac{X_{CH_4,i} - \hat{X}_{CH_4,i}}{X_{CH_4,i}}\right)^2 + \left(\frac{X_{C_2H_6,i} - \hat{X}_{C_2H_6,i}}{X_{C_2H_6,i}}\right)^2\right] \tag{24}$$

Here, N_P is the number of experimental points (training and validation). The set of parameters with the lowest χ^2_{all} (i.e., χ^2_{best}) was selected.

The 5-fold cross validation value (CV_5) is the average value of χ^2_{all} (eq 25). If CV_5 is close to χ^2_{best}, the model is more likely to perform well outside the training region.

$$CV_5 = \frac{1}{5}\cdot\sum_{i=1}^{5}(\chi^2_{all,i}) \tag{25}$$

where $\chi^2_{all,i}$ is the chi-square number for the set of parameters i.

To obtain the confidence interval of each kinetic parameter (CI_i), the standard deviation was calculated considering the five sets of parameters, and then it was multiplied by the two-tail t-student value for 0.05 significance.

Scale-Up of the Proposed Process and Techno-Economic Analysis. This part describes the scale-up process corresponding to the previously described lab-scale plant and the methodology followed for the techno-economic analysis. The chemical plant is assumed to be constructed in Germany. Figure 2 illustrates a simplified process flow diagram with the

https://doi.org/10.1021/acs.iecr.4c01486
Ind. Eng. Chem. Res. 2024, 63, 16683−16700

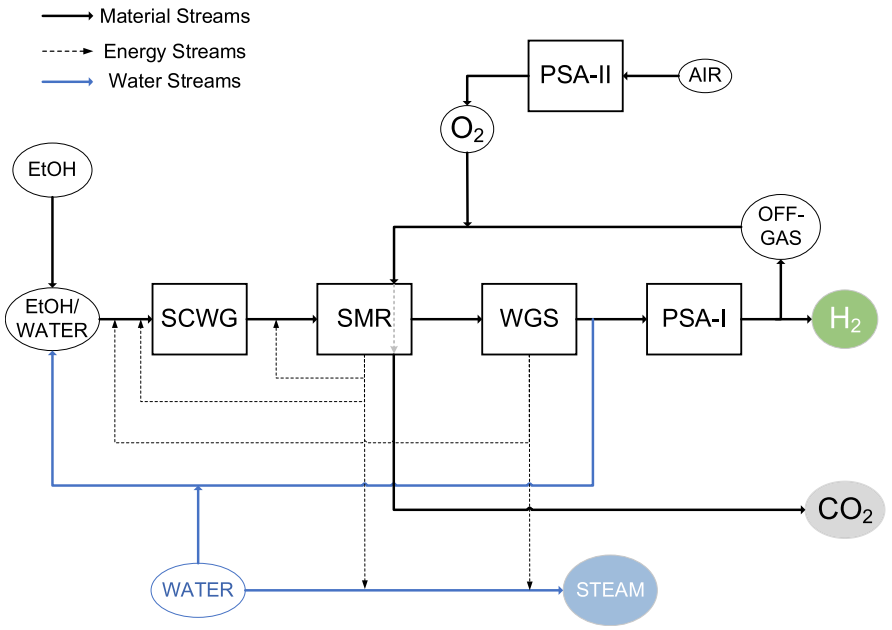

Figure 2. Simplified process flow diagram (PFD) of the scale-up process.

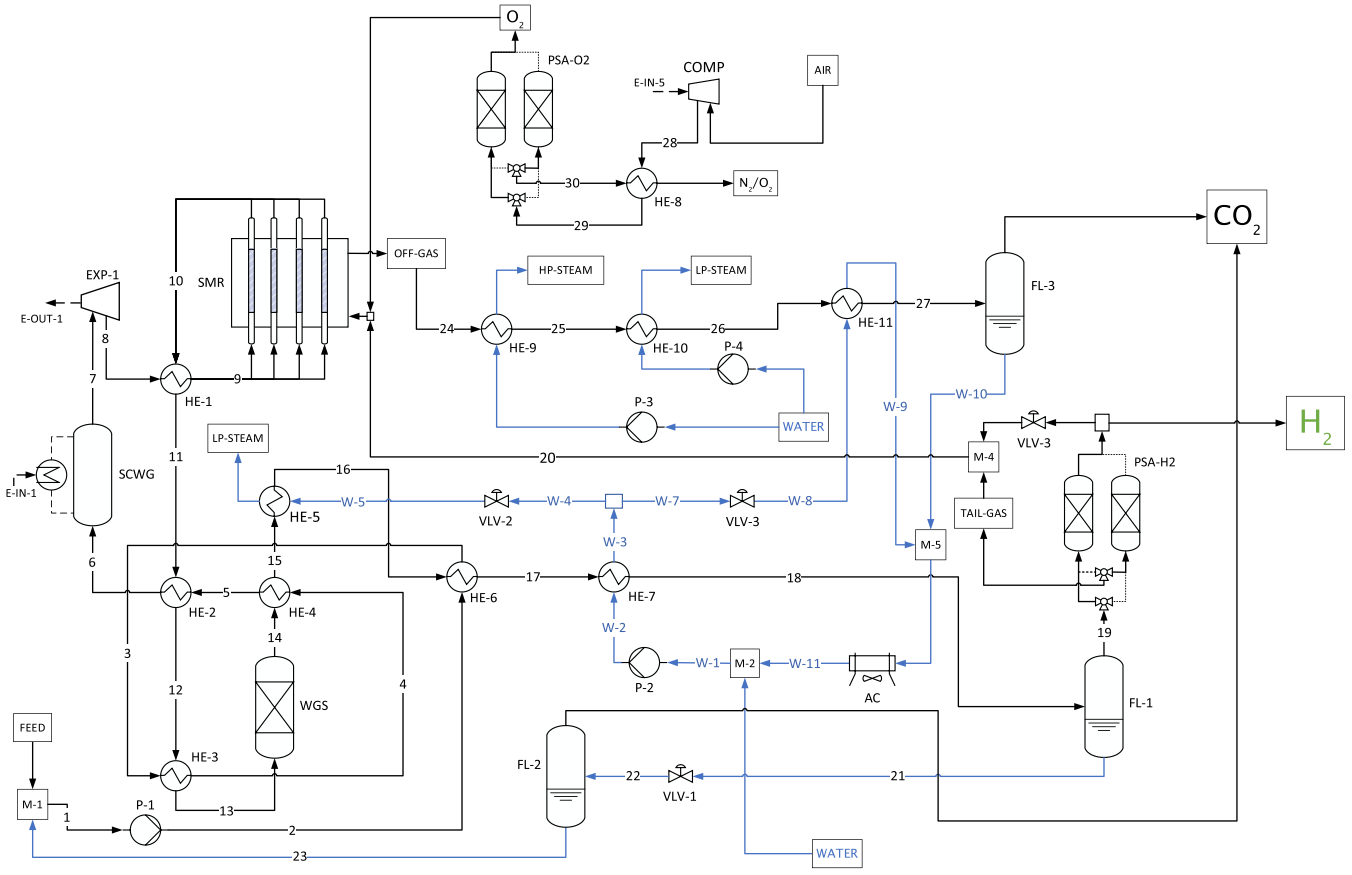

Figure 3. PFD of the scale-up process. The blue arrows indicate the water streams.

main process units and Figure 3 the detailed one. Figure S2 in the Supporting Information (Section S7) presents the process flow diagram as depicted in the Aspen HYSYS software. Table S8 in Supporting Information contains the mass balances, the properties and molar compositions of all the streams from the simulated process in Aspen HYSYS.

The feed to the system is a water−EtOH solution that is pumped to 250 bar (P-1) and preheated to 320 °C (stream 6) prior to SCWG via four heat exchangers. EtOH was used in both cases (experiments and process scale-up) as a biomass model compound establishing a preliminary base case. Gasification

https://doi.org/10.1021/acs.iecr.4c01486
Ind. Eng. Chem. Res. 2024, 63, 16683−16700

takes place at 250 bar and 600 °C. The required heat for the SCWG reactor is provided by electricity.[47]

The product gas, together with the remaining steam (stream 7), is expanded in a turbine (EXP-1) to an outlet pressure of 30 bar (stream 8). Stream 8 is preheated (HE-1) before entering the steam-methane reforming (SMR) reactor. The outlet of the SMR reactor (stream 10) has a temperature of 804 °C and a pressure of 30 bar, providing heat to the inlet of SMR (stream 8) (HE-1).

The product from the SMR is further cooled by heating the feed to the SCWG in HE-2 and HE-3. Afterward, the cooled SMR product is inserted into the WGS adiabatic reactor at around 225 °C. The WGS outlet stream has a temperature increase to approximately 254 °C due to the exothermic WGS reaction.

The product from the WGS reactor is further cooled in HE-4 and HE-6 with the EtOH feed and in HE-5 and HE-7 with water. The heat exchange in HE-5 (heat transferred from stream 15 to W-5) generates low-pressure steam (4.5 bar) that can be sold to nearby industrial facilities.[48] The HE-7 utilizes water (W-2) to cool the WGS product down to 30 °C (stream 18). Afterward, the product gas is separated from condensed water in the gas−liquid separator FL-1. It consists primarily of H_2, CO_2, and traces of CH_4 and CO (stream 19). For the purification of H_2, a PSA unit is implemented. This unit consists of adsorbers filled with zeolite 5A and generates an H_2-rich gas with 99.99% purity and 85% recovery.[49] The recovered water from the product contains a part of the produced CO_2, and it is degassed after pressure reduction close to atmospheric (FL-2), and the released CO_2 is driven to the final CO_2-rich side product (the stream leaving FL-3). Then, the water can be recycled and reintroduced to the feed.

The tail-gas from the PSA unit (stream 20) contains almost all of the CO_2, unreacted CH_4, CO, and part of the produced H_2. It is driven to the SMR oven for oxyfuel combustion to provide the heat required for the SMR reaction system. The oxyfuel combustion is carried out with O_2 separated from N_2 in a PSA unit. There, the air is slightly pressurized by a compressor (COMP) and driven to the PSA unit, where O_2 is recovered at a rate of 53% with a purity of 90%, utilizing a zeolite.[50] The oxyfuel combustion of the tail-gas results in a dry gas consisting primarily of CO_2 (>90 vol. %) that can also be sold. A series of heat exchangers reduce the temperature of the off-gas to 40 °C. From the off-gas cooling, high (25 bar) and low pressure steam (4.5 bar) is generated and sold too. Water is separated from the CO_2 in FL-3 and mixed with the water from the stream W-9. The temperature of this stream is close to 42 °C, and an air-cooled heat exchanger is utilized (AC) to cool it down to 20 °C. Afterward, the cooled water is reintroduced to the system by a pump (P-2).

The scale-up process was simulated with Aspen HYSYS V14. The selected fluid property package was the PRSV, which employs the Peng−Robinson equation of state. A Gibbs reactor was used to simulate the SCWG reaction system by minimizing the Gibb's free energy of the system,[51] which is an adequate approach for this application, as Dutzi et al.[52] demonstrated. They reported complete gasification of EtOH with a concentration ranging from 1.2 to 72 wt %, under 650 °C and 280 bar. The product gas composition was in close agreement with the results from thermodynamic equilibrium when the same process was also simulated with a Gibbs reactor in Aspen HYSYS. Their minimum weight hourly space velocity was 1715 $g_{feed}\ L_{reactor}^{-1}\ h^{-1}$. This value is applied here to design the SCWG reactor, ensuring that the selection of the Gibbs reactor generates satisfactory results in terms of complete carbon gasification efficiency and equilibrium approach.

For accurate simulation of the SMR reactor, a PFR is used in Aspen HYSYS. This unit requires all input related to the kinetic model that was developed in this study. The reactor is considered to be of the multitubular type, with the tubes located inside a furnace. The detailed data for the design of the PFR is given in Supporting Information (see Chapter S7). The furnace (or fired heater) is simulated as a conversion reactor considering the combustion reactions of H_2, CH_4, and C_2H_6. More details regarding the design of this unit can be found in Supporting Information (Chapter S7). An equilibrium reactor was used to model the WGS reactor, considering only the WGS reaction (see Chapter S7 in Supporting Information).

The heat exchangers (HE-1 up to HE-8) were modeled with the Rigorous Shell & Tube model provided by Aspen HYSYS. The gas−liquid separators and the PSA units were designed based on the book by Towler and Sinnott.[53] The specific methodology for both units can be found in Supporting Information (Chapter S7).

An exergy analysis was conducted by determining the exergy efficiency (n_{Ex}, eq 26)[54,55]

$$n_{Ex} = \frac{\dot{m}_{H_2}\cdot e_{H_2} + \dot{m}_{CO_2}\cdot e_{CO_2} + \dot{m}_{steam}\cdot e_{steam}}{\dot{m}_{FEED}\cdot e_{FEED} + P_{electric} + E_Q} \tag{26}$$

where $\dot{m}_i$ is the mass flow rate of stream i, e_i is the specific exergy of the stream I, $P_{electric}$ is the total electric power required by the process operations, and E_Q is the total exergy input for heating purposes. The total exergy loss was calculated as the difference between the inlet exergy streams in the process and the outlet streams.[54] No distinction is made between exergy destruction and exergy loss.[54,55] The specific exergy of a stream (e_i) is calculated as the sum of its physical exergy and its chemical exergy, with the latter being equal to the higher heating value of a material stream (HHV_i, eq 27)[54]

$$\begin{aligned} e_i &= [e_{i,physical}] + e_{i,chemical} \\ &= [H_i - S_i\cdot T_0 - H_i^0 + S_i^0\cdot T_0] + HHV_i \end{aligned} \tag{27}$$

where H_i and S_i are the enthalpy and entropy, respectively, at the actual conditions, H_i^0 and S_i^0 are the enthalpy and entropy at reference conditions (298.15 K and 1 bar), and T_0 is the reference temperature. The physical exergy can be obtained from Aspen HYSYS. The reference conditions were 298.15 K and 1 bar. Table S9 in the Supporting Information enlists the exergy flows of all process streams.

The costs of the equipment (C_i) were calculated from reference equipment costs,[56] considering equipment scaling factors (M) and the effect of inflation on the prices of the equipment based on the chemical engineering plant cost indexes (CEPCI), via the following equation (eq 28)[55]

$$C_i = C_{i,ref}\cdot\left(\frac{Q_i}{Q_{i,ref}}\right)^M\cdot\left(\frac{CEPCI_{2023}}{CEPCI_{ref}}\right) \tag{28}$$

where, Q_i and $Q_{i,ref}$ are the characteristic capacities and M is the equipment scaling factor.[56] The prices of the equipment were corrected to 2023 with the corresponding value of CEPCI for May 2023, which is 808.8.[57] The values of $CEPCI_{ref}$ varied according to the available source of reference equipment.

https://doi.org/10.1021/acs.iecr.4c01486
Ind. Eng. Chem. Res. 2024, 63, 16683−16700

The total cost of the main equipment (C_{total}), multiplied by the Lang Factor (F_L), corresponds to the fixed capital investment (CI_{fixed}, eq 29)

$$CI_{fixed} = F_L \cdot C_{total} \quad (29)$$

where C_{total} accounts for the sum of all main equipment costs

$$C_{total} = \sum C_i \quad (30)$$

The Lang factor is frequently used to obtain order-of-magnitude cost estimates and takes into account the direct and indirect costs related to the construction of tP, based on the equipment costs.[56] The Lang factor was estimated to be 4.86, according to Albrecht et al.[58] Table S13 in the Supporting Information contains all the different cost types that contributed to the CI_{fixed}. The total capital investment (CAPEX) was calculated by the following equation (eq 31)[55]

$$CAPEX = CI_{fixed} + C_{working} \quad (31)$$

where $C_{working}$ stands for the working capital. According to Peters et al.[56] the $C_{working}$ lies between 10 and 20% of CAPEX. In this work, a value of 15% of the CAPEX was selected.

The annual capital costs (C_a) can be given as a function of the CI_{fixed} and $C_{working}$, based on the annuity method (eq 32)[55]

$$C_a = \frac{CI_{fixed} \cdot r \cdot (1+r)^{t_p}}{(1+r)^{t_p} - 1} + r \cdot C_{working} \quad (32)$$

where r is the annual interest rate, assumed equal to 10%, and t_p is the operating lifetime of the plant which was considered to be 20 years.[59] No salvage value was considered.

The direct and indirect operating expenses ($OPEX_{dir}$ and $OPEX_{ind}$, respectively) were also estimated. The $OPEX_{dir}$ correspond to the costs of EtOH, cooling and clean water, electricity, catalysts for SMR and WGS, and adsorbents for the PSA units. Table 1 presents the unit costs of all the aforementioned utilities and the prices of the products to be sold, i.e., low pressure and high pressure steam and CO_2. The $OPEX_{ind}$ consist of costs associated with operating labor, operating supervision, maintenance labor, maintenance materials, operating supplies, laboratory expenses, insurance, taxes, plant overhead, administrative costs, distribution and selling, research and development. The methodology of calculating them was taken from Albrecht et al.[58]

Table 1. Unit Costs of Purchased Utilities and of Products for Sale

utility	unit cost	references
unit costs of utilities constituting the $OPEX_{dir}$		
EtOH	0.56 \$ L^{-1}	60
cooling water	0.0013125 \$ m^{-3}	58
clean water	2.1 \$ m^{-3}	58
electricity	0.0945 \$ kWh^{-1}	58
SMR catalyst	29.7 \$ kg^{-1}	61
WGS catalyst	19 \$ kg^{-1}	55
adsorbent of PSA-H_2	2.0 \$ kg^{-1}	59
adsorbent of PSA-O_2[a]	2.0 \$ kg^{-1}	59
unit costs of products to be sold		
low-pressure steam (4 bar)	27.0 \$ t^{-1}	58
high-pressure steam (25 bar)	27.6 \$ t^{-1}	58
CO_2	46.5 \$ t^{-1}	55

[a]No price for adsorbents in the PSA-O_2 was found in the literature, thus it was assumed that the price for a PSA-O_2 adsorbent is same with that of the adsorbent in the PSA-H_2 unit.

The operating labor costs (C_{OL}) were calculated according to the following equation (eq 33)

$$C_{OL} = Wage_{OP} \cdot N_{OP} \quad (33)$$

where the $Wage_{OP}$ is the wage of every operator, equal to 72.000 € a^{-1}[55] (or 75.600 $\$_{2023}$ a^{-1}), and N_{OP} is the total number of operators calculated by 34[55,62]

$$N_{OP} = F_{OP} \cdot [(6.29 + 0.23 \cdot N_{np})^{0.5}] \quad (34)$$

where N_{np} is the number of nonparticulate processing units in the scaled-up plant, and F_{OP} the number of operators to cover every position in the plant at any time, which was estimated to be 4.5. A description on how C_{OL} is estimated at different plant capacities, is given in Supporting Information (S8). As the plant scales up, labor costs increase. Peters and Timmerhaus provide in their book[56] a diagram through which one can estimate the operating labor requirements when the capacity of the chemical plant increases.

The net production costs (NPC) can be estimated in \$ a^{-1} (eq 35). The break-even price of H_2 is also calculated, taking into account the sale of CO_2 and steam of low and high pressure (LP and HP, respectively) as follows (eq 36)

$$NPC(\$ \cdot a^{-1}) = C_a + OPEX_{dir} + OPEX_{ind} \quad (35)$$

$$P_{BE}(\$ \cdot kg_{H_2}^{-1}) = \frac{NPC - (\dot{m}_{CO_2} \cdot C_{CO_2} - \dot{m}_{steam_{LP}} \cdot C_{steam_{LP}} - \dot{m}_{steam_{HP}} \cdot C_{steam_{HP}})}{\dot{m}_{H_2}} \quad (36)$$

All assumptions applied for the economic analysis are given in Table 2.

Table 2. Assumptions Used for the Economic Analysis

assumption number	parameter	value
1	working capital ($C_{working}$)	15% of CAPEX
2	annual interest rate (r)	10%
3	operating lifetime of the plant (t_p)	20 years
4	hours of operations in a year	8000 h a^{-1}
5	average labor costs	75,600 \$ a^{-1}
6	number of nonparticulate processing units in the chemical plant (N_{OP})	3
7	number of operators to cover every position in the plant at any time (F_{OP})	4.5

RESULTS AND DISCUSSION

Kinetic Modeling of SMR and SER. *Kinetic Model Parameters and Performance.* In both Models M1 and M2, the optimization procedure gave $K_{CH_4} = 0$. Besides, in model M2, k_1 and K_{H_2O} were growing together to extremely large values, indicating a high correlation between them and suggesting the following change from eqs 15−37

$$K_{H_2O} \cdot p_{H_2O} \cdot p_{H_2}^{-1} \gg 1 + K_{CH_4} \cdot p_{CH_4} \rightarrow \theta_* \approx (K_{H_2O} \cdot p_{H_2O} \cdot p_{H_2}^{-1})^{-1} \quad (37)$$

https://doi.org/10.1021/acs.iecr.4c01486
Ind. Eng. Chem. Res. 2024, 63, 16683−16700

With this consideration in model M2, K_{H_2O} could be lumped to the kinetic constants, reducing the number of parameters to four (see mathematical demonstration in Section S3). A similar approach was also tested for models M1 and M3 for comparison purposes. In the end, the total number of developed models was extended to five: (i) M1 (4 parameters), (ii) M1 (5 parameters), (iii) M2 (4 parameters), (iv) M3 (4 parameters), and (v) M3 (6 parameters). In Table 3, the statistic values of all models are presented. The mean error of methane and ethane conversion were calculated as follows (eq 38)

$$\mathrm{ME} = \frac{1}{N_\mathrm{p}} \cdot \sum_{i=1}^{N_\mathrm{p}} \left| \frac{X_i - \widehat{X}_i}{X_i} \right| \tag{38}$$

Table 3. Statistical Performance Indicators

	M1 (4p)	M1 (5p)	M2 (4p)	M3 (4p)	M3 (6p)
χ^2_{best}	0.849	0.801	0.873	0.633	0.291
CV_5	0.909	0.874	0.953	0.651	0.327
ME-X_{CH_4} (%)	15.8	16.1	17.7	13.1	9.0
ME-$X_{C_2H_6}$ (%)	4.6	4.7	4.6	4.6	4.7

Model M3 (6p) outperforms all other models, with its χ^2_{best} being 50% lower than model M3 (4p), the second best model, and around 70% lower than models M1 and M2. The average errors of model M3 (6p) are significantly low: 9.0 and 4.7% for K_{CH_4} and $X_{C_2H_6}$, respectively. Furthermore, CV_5 of all models are close to their χ^2_{best}, indicating adequate simulation outside the training region. Since the performance of model M3 (6p) was much superior than the other models, it is chosen for further analysis and for the process simulation. In Table 4, the parameters and all equations of model M3 (6p) are summarized. The parameters and equations of the other models are provided in the Supporting Information (Chapter S4).

In Figure 4, experimental and simulated values of CH_4 and C_2H_6 conversion are shown as functions of temperature (Figure 4a,b), space velocity (Figure 4c,d), and pressure (Figure 4e). C_2H_6 conversion as a function of pressure is not shown because either complete conversion or almost complete conversion was reached in all cases. While all models reasonably reproduce the experimental data for the different variations in operating conditions, model M3 (6p) clearly outperforms the other models, especially with regards to CH_4 conversion for temperature and pressure variations.

Table 4. Summary of Equations and Parameters of Model M3 (6p)[a]

equation or variable		refs
SMR to CO: $r_1 = k_1 \cdot \theta_*^2 \cdot \left(\frac{p_{CH_4} \cdot p_{H_2O}}{p_{H_2}^2} - \frac{p_{H_2} \cdot p_{CO}}{K^0_{P,1}} \right)$		eq 14
WGS: $r_3 = k_3 \cdot \theta_*^2 \cdot \left(\frac{p_{CO} \cdot p_{H_2O}}{p_{H_2}} - \frac{p_{CO_2}}{K^0_{P,3}} \right)$		eq 10
SER: $r_4 = k_4 \cdot p_{C_2H_6}$		eq 17
$k_i = \exp\left[A_i - \frac{E_{A_i}}{R} \cdot \left(\frac{1}{T} - \frac{1}{873.15} \right) \right]$		eq 12
$\theta_* = (1 + K_{CH_4} \cdot p_{CH_4} + K_{H_2O} \cdot p_{H_2O} \cdot p_{H_2}^{-1})^{-1}$		eq 15
$A_1 = -2.125 \pm 1.011$	$E_{A_1} = (37.86 \pm 10.63)$ kJ·mol^{-1}	
$A_3 = 5$	$E_{A_3} = 0$ kJ·mol^{-1}	*[b]
$A_4 = 0.498 \pm 0.078$	$E_{A_4} = (14.61 \pm 3.99)$ kJ·mol^{-1}	
$K_{CH_4} = (2.996 \pm 1.529)$ bar^{-1}	$K_{H_2O} = 0.419 \pm 0.392$	

[a]The reaction rates are given in mol kg_{cat}^{-1} s^{-1}. [b]WGS parameters were chosen to give a high reaction constant, so that this reaction is in quasi-equilibrium.

The experiments from the temperature variation (Figure 4a) suggest a sinusoidal behavior, while the curves from most models were significantly softened, almost linear in some cases. model M3 (6p) had the best fit, probably aided by the adsorption components. This sinusoidal behavior from the experiments might indicate temperature dependent adsorption, in which higher temperature improve desorption, enhancing the fraction of free sites, and, therefore, the reaction rates. The addition of such parameters might further improve model M3 (6p), but more experiments would have to be performed for all parameters to remain statistically significant.

Pressure has a known negative effect on the SMR rates of all models related to thermodynamics, as the number of mols increases within the reaction. Besides, models M1 and M2 include a negative effect of pressure related to kinetics ($r \propto p^{-0.5}$), which is apparently too strong and should be the cause of the systematic X_{CH_4} underestimations in Figure 4e. Model M3 (4p) gave moderate X_{CH_4} overestimations, which were fairly corrected by the addition of the adsorption parameters, i.e., in model M3 (6p) curve. Still, the experimental results show a stabilization after 25 bar, probably because a poisoning phenomenon from one of the substances (probably H_2O or CH_4) reached a saturation point, which model M3 (6p) could not perfectly reproduce. A further improvement of the model might be possible by performing further experiments, expanding the parameter number (e.g., with K_{CO} and/or K_{H_2}) and re-estimating the parameters.

Finally, in Figure 4f parity plots of model M3 (6p) simulations are presented. All points are between the ±20% lines, indicating excellent agreement between experiments and simulations. The parity plots of all models can be found in the Supporting Information (Chapter S5).

Checking the Influence of Mass Transfer Phenomena. The activation energies of the steam reforming reactions of the models developed in this work were lower than typical literature models (134 to 240 kJ mol^{-1}).[41,63,64] The question was raised if mass transfer phenomena in the experiments could be limiting the reaction. The possible influence of external and/or internal mass transfer phenomena on the reaction rates during the experiments was determined by applying three criteria. To check for possible external mass transfer effects the Mears criterion was applied (eq 39)[65]

$$M_\mathrm{criterion} = \frac{r_\mathrm{A} \cdot \rho_\mathrm{b} \cdot R \cdot n}{k_\mathrm{c} \cdot C_{\mathrm{A(bulk)}}} \ll 0.15 \tag{39}$$

where r_A is the reaction rate of the limiting reactant (mol kg_{cat}^{-1} s^{-1}), ρ_b the catalyst's apparent density (kg m^{-3}), R the radius of the catalyst particles (m), n the reaction order, k_c the gas-particle mass transfer coefficient (m s^{-1}), and $C_{A(bulk)}$ the reactant's concentration in the bulk gas phase (mol m^{-3}). For internal mass transfer limitations, the Weisz−Prater criterion was used (eq 40)[66]

https://doi.org/10.1021/acs.iecr.4c01486
Ind. Eng. Chem. Res. 2024, 63, 16683−16700

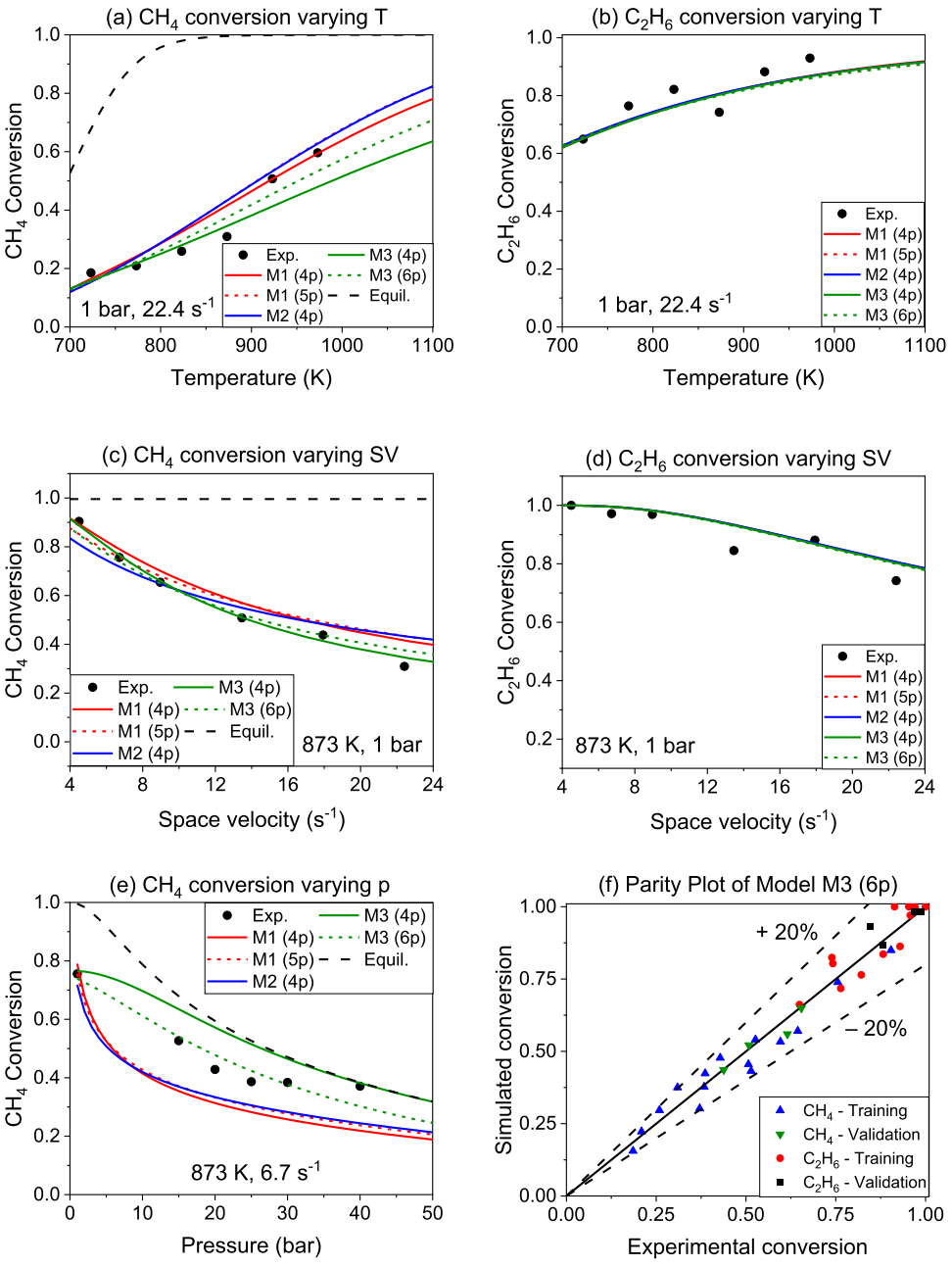

Figure 4. Experimental and predicted values of CH_4 and C_2H_6 conversion under different conditions of temperature (a,b), space velocity (c,d), and pressure (e). In (f) parity plots of model M3 (6p) for all conditions are shown.

$$\mathrm{WP}_{\mathrm{criterion}} = \frac{r_A \cdot \rho_c \cdot R^2}{D_{\mathrm{eff.}} \cdot C_{A(\mathrm{surface})}} \ll 1 \tag{40}$$

where ρ_c the catalyst's density (kg m^{-3}), $D_{\mathrm{eff.}}$ the effective diffusivity (m^2 s^{-1}), and $C_{A(\mathrm{surface})}$ the concentration of the reacting gas on the catalyst surface (mol m^{-3}). Furthermore, for the internal mass transport phenomena, the effectiveness factor, i.e., the ratio of the actual reaction rate to the one if the activity of the catalyst was uniform throughout the catalyst particles (in the kinetic regime), was determined assuming spherical catalytic particles (eq 41)[67]

$$\eta = \frac{3}{\varphi}\left(\frac{1}{\tanh(\varphi)} - \frac{1}{\varphi}\right) \tag{41}$$

The parameter φ in eq 41 represents the Thiele modulus that compares the chemical reaction rate to the rate of intraphase diffusion (eq 42)[67,68]

$$\varphi = R \cdot \sqrt{\frac{c}{D_{\mathrm{eff.}} \cdot R_h}} \tag{42}$$

R is the radius of the spherical particles in m, $D_{\mathrm{eff.}}$ is the effective diffusivity in m^2 s^{-1}, R_h is the hydraulic radius of the pores, calculated by dividing the total pore volume (m^3 $kg_{cat.}^{-1}$) by the catalyst surface area, A_p (m^2 $kg_{cat.}^{-1}$). The parameter c (m s^{-1}) is the reaction rate of SMR (r_A) divided by the methane bulk concentration, C_{CH_4} (mol m^{-3}), and the A_p.[67] Information regarding their calculation can be found in Supporting Information (S6.2).

https://doi.org/10.1021/acs.iecr.4c01486
Ind. Eng. Chem. Res. 2024, 63, 16683−16700

With regard to the external mass transfer control, the highest calculated value of the Mears criterion was $6.71 \times 10^{-4} \ll 0.15$, indicating no control by external mass diffusion. On the other hand, the Weisz−Prater criterion values were in the range 0.18−0.30 at ambient pressure and 600 °C. Under the same pressure but higher temperatures, the values of the criterion increased, reaching a value of 0.66 at 700 °C. The respective values dropped 1 order of magnitude as the pressure increased to 10 bar. From 10 to 40 bar (at 600 °C and 22,234 h^{-1}) the value of the criterion dropped from 0.017 to 0.0081. Similarly, the effectiveness factor η ranged from 0.79 to 0.93 under ambient pressure and temperatures between 600 and 700 °C. Higher pressures resulted in $\eta > 0.99$. These results suggest that under atmospheric pressure, temperatures in the range of 450 −700 °C, and GHSV ranging from 14,852 to 74,163 h^{-1}, intraphase diffusion may affect the reaction rates, possibly due to the very low partial pressure of methane in the feed (0.033 atm) and at the same time due to the low total pore volume of the catalyst. The numerical values of each criterion in all experimental conditions can be found in the Supporting Information (Chapter S6).

Checking the Influence of Nonidealities in the Gas Phase. The kinetic model was developed assuming ideal gas (IG) behavior. In order to check if nonidealities are significant in our operating region of interest, the following test was performed: the block RGIBBS from Aspen Plus was used to calculate the chemical equilibrium for a range of pressures and temperatures. The inlet feed mass composition was: H_2O = 81.999%, CH_4 = 6.400%, CO = 0.200%, CO_2 = 10.700%, H_2 = 0.700%, C_2H_6 = 0.001%. Simulations were performed for both IG and Peng−Robinson (PR) equations of state, and the results are shown in Figure 5. The influence of nonidealities in the gas phase is in general not significant, growing with increasing pressure and decreasing temperature (as expected). At 30 bar, the deviation is only 0.01 at 773 and 923 K while a mere 0.002 at 1073 K.

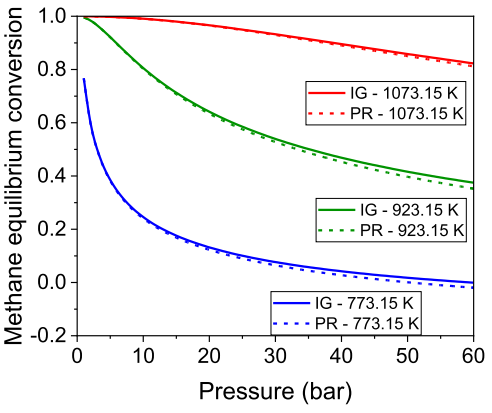

Figure 5. Simulation of chemical equilibrium in the SMR considering IG and Peng−Robinson (PR).

Implementation of the Kinetic Model to the SMR Reactor in the Scale-Up Process. The kinetic model M3 was applied in Aspen HYSYS to simulate the SMR reactor as a PFR reactor. Here, a description of its performance and operational parameters is given for one of the critical cases systematically reported in the economic analysis, i.e., feed flow rate of 10 t h^{-1} and 15 wt % EtOH concentration. The SMR's outlet temperature and pressure were fixed at 804 °C and 30 bar, respectively. In this case, the required heat input was equal to 3227 kW. The reactor's volume was calculated to be equal to 0.5 m^3, while GHSV = 26,220 h^{-1}. According to Nielsen et al.,[21] the GHSV used in industrial applications is typically around 2000−4000 h^{-1}. Such a higher space velocity is possible due to the very high H_2O/CH_4 ratio of this study, driving the SMR reaction toward H_2 formation,[14,69] which in this case was equal to 11.3, compared to a conventional SMR reactor, operating at H_2O/CH_4 ratios = 2.5−3.[16,21,70] Besides, the desired CH_4 conversion accounted for 74.4%, without the need of lower GHSV (i.e., longer residence times). Additional design characteristics can be found in the Supporting Information S7.

Figure 6 illustrates the temperature profile and the reaction rates in the SMR reactor along the tubes' length, and Figure 7 shows the dry product gas composition. The SMR reaction rate has its highest value of 25 mol m^{-3} s^{-1} at the inlet, decreasing gradually to approximately 5 mol m^{-3} s^{-1} at the reactor's outlet. The WGS reaction rate follows the same trend but close to the tube's end, where the temperature reaches 750 °C, it reaches zero and then becomes negative, designating the promotion of the reverse WGS.

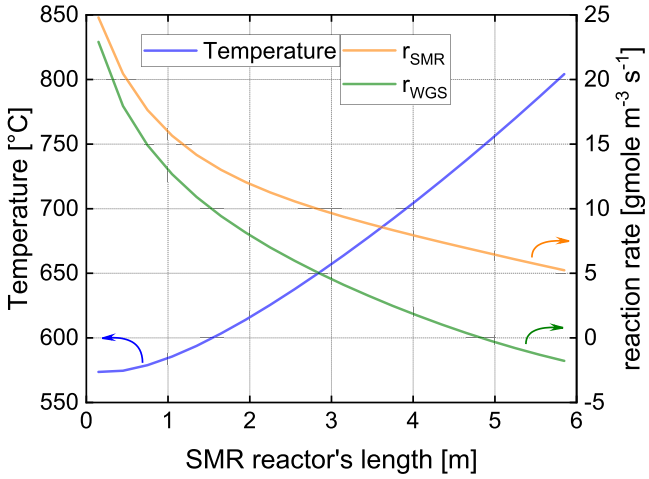

Figure 6. Profile of temperature and rates of reactions in the SMR reactor. The data correspond to the simulation with 15 wt % EtOH in the feed with 10 t h^{-1} rate. The temperature of outlet stream of the SMR is 804 °C and the pressure 30 bar.

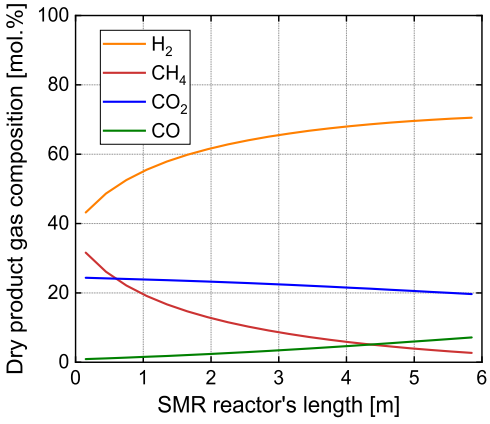

Figure 7. Profile of dry product gas composition along the SMR reactor. The data correspond to the simulation with 15 wt % EtOH in the feed with 10 t h^{-1} rate. The temperature of outlet stream of the SMR is 804 °C and the pressure 30 bar.

https://doi.org/10.1021/acs.iecr.4c01486
Ind. Eng. Chem. Res. 2024, 63, 16683−16700

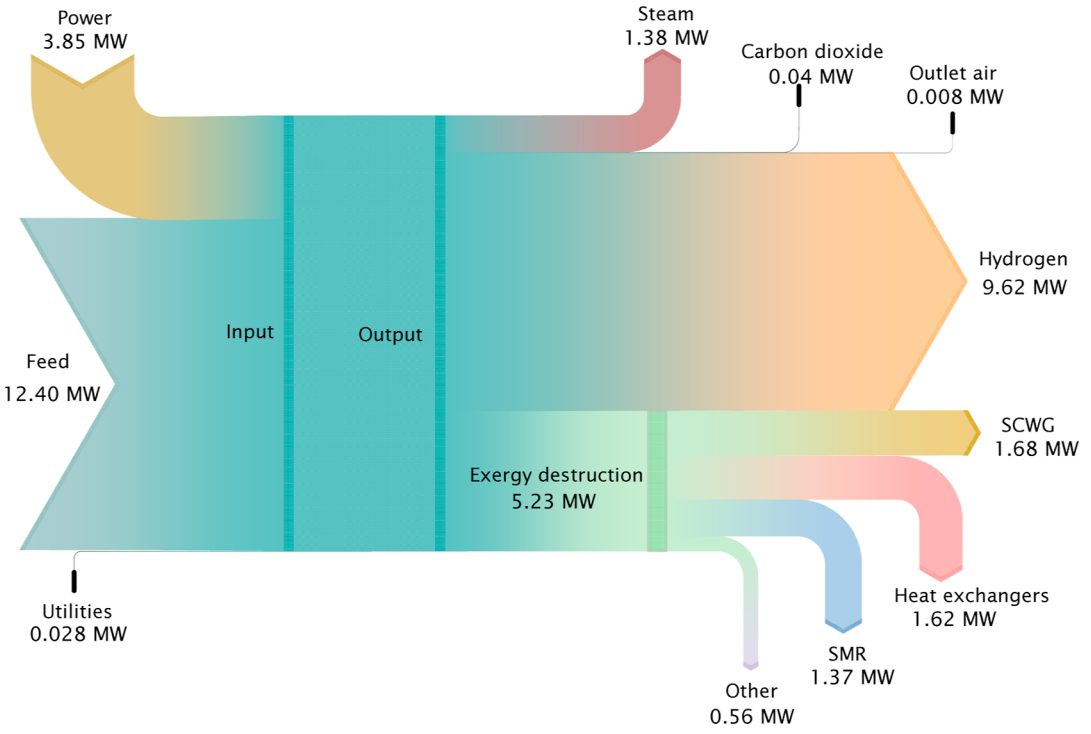

Figure 8. Exergy balances for the case of 15 wt % EtOH with a feed flow rate of 10 t h^{-1}.

The temperature of the reactor's inlet is low because the feed enters at 578 °C, but gradually increases along the length of the reactor. The SMR reaction rate strongly depends on the temperature of the reactor. The SMR reaction proceeds faster, closer to the inlet, where the amount of methane is larger, consuming more energy due to its endothermic nature. Gradually, as the methane decreases, the energy supplied becomes more and more sufficient to heat the reactor and promote methane steam reforming.[64] Similarly, the elevation of H_2 concentration and the reduction in CH_4 concentration, as depicted in Figure 7, are steeper closer to the reactor's inlet, gradually attenuating as they approach the reactor outlet.

Exergy Analysis. For the exergy analysis, the same case with 15 wt % ethanol in the feed and a feed flow rate of 10 t h^{-1} was considered. Figure 8 shows the overall exergy balance. The total exergy input was 16.28 MW, with the process feed and the electric power input contributing 76.18 and 23.65% of it, respectively. Hydrogen accounted for the largest portion of the exergy output, representing 59.09% of the exergy input. The exergy efficiency, calculated using eq 26, was estimated to be 67.8%.

The total exergy destruction was 5.23 MW. The SCWG reactor accounted for the largest share of the total exergy destruction, at 32.13%, primarily due to the significant amount of electricity required for heating. The heat exchangers followed, contributing 30.98% to the total exergy destruction. These heat exchangers were used to preheat the feeds to the SCWG and SR reactors by cooling their product streams, cool the final H_2-rich product, and cool the off-gas from the fired heater in the steam reformer. The latter two tasks involved generating low- and high-pressure steam across large temperature differences.

The steam reformer was the third largest contributor to exergy destruction, at 26.27%, due to the combustion of some of the produced hydrogen and unreacted hydrocarbons to provide heat for the SR reactions, resulting in the production of CO_2,H_2O, and thermal energy. The remaining exergy losses were attributed to other process units, such as the WGS reactor, the PSA units, the expander, and the air compressor.

Techno-Economic Analysis. Section S7 in Supporting Information provides the mass balances and the molar composition of all the streams used in the simulation, for the case of 15 wt % EtOH and 10 t h^{-1}. The equipment costs for this case are given in Section S8, together with the total equipment costs for different EtOH concentrations (Table S11) and different feed flow rates (Section S12). Section S8 also enlists the capital investments for every different simulated case.

Effect of EtOH Concentration on the Break-Even Price of H_2. Figure 9 shows the break-even price of produced hydrogen, the ratios of NPC and H_2 production to their value for 8 wt % EtOH as a function of the feed concentration. A significant decrease in the P_{BE} is found from 8 to 18.5 wt % of EtOH concentration. More specifically, the P_{BE} for 8 wt % EtOH accounts for 40.1 \$ $kg_{H_2}^{-1}$, whereas at 18.5 wt % EtOH, the P_{BE} drops to 18.9 \$ $kg_{H_2}^{-1}$. A further increase in the EtOH

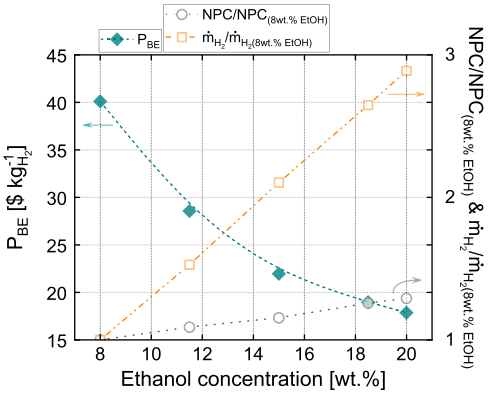

Figure 9. Break-even price of hydrogen with EtOH concentration in the feed. The feed flow rate is 1 t h^{-1}.

https://doi.org/10.1021/acs.iecr.4c01486
Ind. Eng. Chem. Res. 2024, 63, 16683−16700

concentration leads to slighter drop in the P_{BE}, e.g., for 20 wt % EtOH, the P_{BE} was calculated to be equal to 17.9 \$ $kg_{H_2}^{-1}$. Both H_2 production and NPC rates increase linearly with EtOH concentration, but that of H_2 is significantly greater than that of NPC. Considering therefore the eq 36 of P_{BE} and that the contributions of the LP-steam, HP-steam, and carbon dioxide terms are small, the drop in the hydrogen value with ethanol concentration is justified by the curve in Figure 9. The feed concentration of the organics thus, plays a crucial role in the profitability of this process. Fang et al.[71] designed and simulated a SCWG plant for the gasification of 15 and 25 wt % glucose, and 15 wt % sewage sludge with a feed flow rate of 30 t h^{-1}. They estimated that their process became profitable, in terms of annual net income, when hydrogen had a minimum selling price of around 4 \$ $kg_{H_2}^{-1}$ for 25 wt % glucose and 5 \$ $kg_{H_2}^{-1}$ for 15 wt % glucose, respectively.

Higher biomass concentrations can lead to technical bottlenecks in the operation of continuous processes. The carbon gasification yield decreases with increasing biomass concentration, leaving more carbonaceous products as side products in the liquid effluent (tar and char) or as solid deposits.[4,8,13] A high concentration of such organic byproducts in the liquid effluent can cause clogging[72] and also can poison the downstream SMR catalyst.[73] Boukis and Stoll[13] argued that a positive energy balance and relatively high yield of product gas can be generated when the feed concentration lies between 8 and 12 wt % of dry matter. Previous experiments from the same group[13] with corn silage at 700 °C and 250 bar had shown that an increase in the biomass concentration from 5 to 19 wt % leads to a reduction in the carbon gasification yield from almost 100 to 80%, respectively, and a rise in the total carbon content in the effluent from around 750 ppm, at 5 wt %, to approximately 2600 ppm at 20 wt %. Given this technical limitation faced by the SCWG of real biomass types, and considering the results of the Figure 9, the EtOH concentration chosen for further study was 15 wt %.

Effect of Feed Flow Rate on the Break-Even Price of H_2. The effect of the feed flow rate on the H_2 break-even price is shown in Figure 10a. There is a steep decline in the P_{BE} from 22.0 \$ $kg_{H_2}^{-1}$, at 1 t h^{-1}, to 9.0 \$ $kg_{H_2}^{-1}$, at 10 t h^{-1}. An increase to 50 t h^{-1} results in a slighter drop in the P_{BE} price to 6.8 \$ $kg_{H_2}^{-1}$. A further increase in the feed flow rate does not significantly improve P_{BE}, leading to a final price of 6 \$ $kg_{H_2}^{-1}$ at 160 t h^{-1}. Figure 10b compares the NPC and their constituents for different feed flow rates. The NPC at 160 t h^{-1} are 51 times higher than the NPC at 1 t h^{-1}. What also stands out is the high increase rate of the $OPEX_{dir}$ with feed flow rate, compared to the C_a and $OPEX_{ind}$. Despite the large increase in production costs, the price of hydrogen tends to reach a stable price in the range studied, consistent with the economies of scale.[25]

These results are similar to those of Kumar et al.,[25] who found that a higher feed flow rate than 83.3 t h^{-1} in a SCWG process of microalgae would not yield further decrease in the price of H_2, which at that point was around 4.6 \$ $kg_{H_2}^{-1}$. The latter price from Kumar et al.[25] at 83.3 t h^{-1} is lower than even the P_{BE} price of this study at 160 t h^{-1}. This difference is attributed to the high price of EtOH that was used here, i.e., 707 \$ t_{EtOH}^{-1}, compared to the price of the algal biomass from Kumar et al.,[25] i.e., 392 \$ t^{-1} of dry biomass. Campanario and Gutiérrez Ortiz[24] studied the effect of plant capacity from 20 to 200 t h^{-1} in the process of bio-oil aqueous phase SCWG coupled with WGS, dry reforming and Fischer−Tropsch (FT) synthesis. The selling prices of the FT-biofuels had been halved from 20 to around 90 t h^{-1}, e.g., the price of gasoline decreased from 2.1 \$ kg^{-1} to around 1.1 \$ kg^{-1}. After this range, the decrease was less significant.

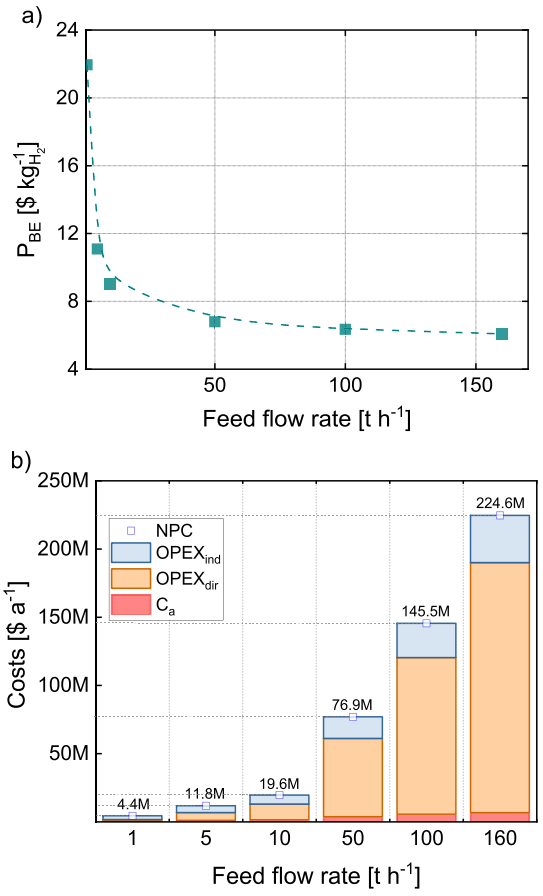

Figure 10. (a) Break-even price of hydrogen with varying feed flow rate, (b) NPC in \$ a^{-1} and its components with feed flow rate. The concentration of EtOH in the feed is 15 wt %.

As can be seen from Figure 11, EtOH costs are the most significant contributor to $OPEX_{dir}$, followed by electricity. It is also apparent from Figure 11 that the distribution of costs remains almost the same with increase in feed flow rate.

Based on Figure 10a, a feed flow rate of 50 t h^{-1} can be sufficient to improve the profitability of this process, as described above. Above this scale, the availability of different feedstocks should be considered to determine a suitable plant size. For example, Campanario and Gutiérrez Ortiz[24] proposed a theoretical optimum plant capacity for the processing of bio-oil aqueous phase in SCWG to be around 200 t h^{-1}, after which the reduction in production costs is negligible in their proposed process chain. However, they argued that a more realistic capacity should aim at 100 t h^{-1} due to feedstock availability. One relevant feedstock for the proposed process in this article is sewage sludge, as it is a wet feedstock that does not need to be dried in SCWG and thus can be energetically utilized very efficiently.[13,15,35,74,75] According to Fang et al.,[71] a sewage sludge flow rate of 30 t h^{-1} with 15 wt % dry biomass corresponds to the disposal capacity of a city with around 1.3 million citizens. Similarly, a flow rate of 50 t h^{-1} would correspond to a city of 2.16 million citizens. As an example, this roughly corresponds to the number of citizens of Hamburg, Germany.[76] As this is the second largest city in Germany, a capacity higher than 50 t h^{-1} of

https://doi.org/10.1021/acs.iecr.4c01486
Ind. Eng. Chem. Res. 2024, 63, 16683−16700

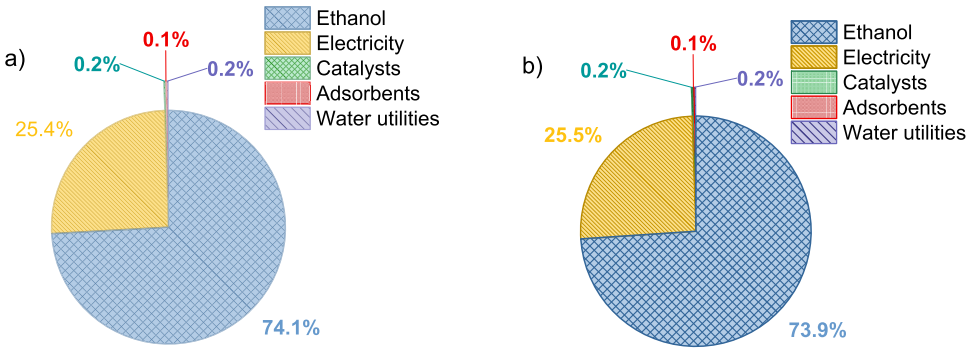

Figure 11. Component cost allocation of direct operating expenditures ($OPEX_{dir}$) for the case of 15 wt % EtOH with (a) 10 and (b) 50 t h^{-1}.

sewage sludge would not be meaningful in this country. Another suitable feedstock is glycerol, which can be easily gasified and is a cheap educt.[77−80] According to Attarbachi et al.,[81] the supply of glycerol will exceed demand by about 2.33 million tons by 2025. Assuming that the proposed process uses 15 wt % glycerol with a capacity in the range of 10 to 50 t h^{-1} of total feed flow rate, it will process about 0.5 to 2.6% of the world's total glycerol surplus by 2025. In conclusion, for the proposed process, a maximal capacity of 50 t h^{-1} should be reached in order to increase sufficiently its profitability.

Sensitivity Analysis. A sensitivity analysis of specific parameters that affect the P_{BE} was carried out. The analysis was based on a feed flow rate of 10 t h^{-1}. The investigated parameters were the unit prices of EtOH, electricity, and clean water, the total purchase cost of equipment, and the operating labor costs. Each parameter varied from their reference value by ±50%, while the others remained constant. The results are summarized in Figure 12. The price of EtOH seems to have the

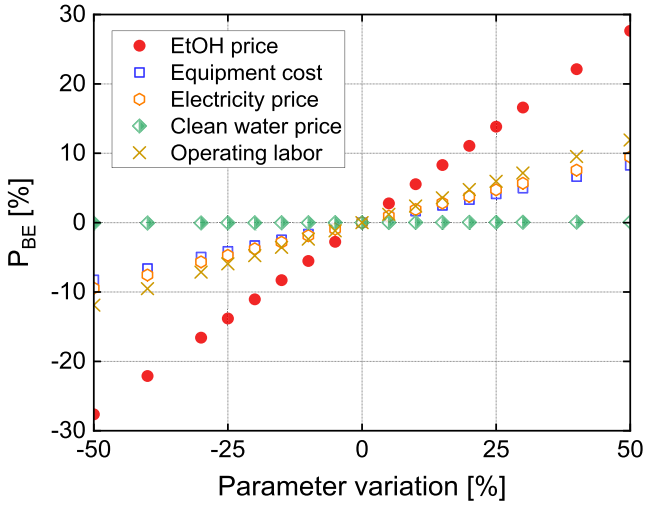

Figure 12. Effect of the percentage changes in the price of various parameters on P_{BE}, for the case of 15 wt % EtOH with 10 t h^{-1} feed flow rate.

most significant effect on the P_{BE}, with a ±50% change in its value resulting in a 27.6% variation in P_{BE} (i.e., 6.5−11.5 \$ $kg_{H_2}^{-1}$). Kumar et al.[25] found that a 20% variation in the cost of algae leads to a change slightly higher than 20% in the hydrogen value. Galera and Gutiérrez Ortiz[77] varied the price of glycerol up to 50% in an SCWG process with a 1 t h^{-1} glycerol flow rate with around 26.5 wt % concentration, coming up with a hydrogen selling price variation of around 17%. Gasafi et al.,[75] who studied the SCWG of sewage sludge with 5 t h^{-1}, assuming a negative unit feedstock cost, estimated that an increase of 50% in sludge revenue would reduce hydrogen production costs by 72%.

Following the effect of EtOH price, the operating labor brings about a variation in P_{BE} of 11.9%. The equipment costs and the price of electricity cause a roughly similar change in the price of hydrogen, i.e., 8.3 and 9.5%, respectively. The price of clean water had a negligible impact on the break-even price of H_2. These results suggest a significant reduction in the break-even price of hydrogen can be achieved by reducing the price of ethanol. Since ethanol was used as the biomass model in this study, it is reasonable to examine the effect of its price on P_{BE} in more detail, thus representing different biomass types.

Effect of the EtOH Price on the Break-Even Price of H_2. The last chapter of the techno-economic analysis focuses on the effect of the EtOH price on the hydrogen break-even price. Therefore, the two case studies, which represent the technically feasible operation range in feed flow rate, i.e., 10−50 t h^{-1}, were regarded. In both cases, the price of EtOH varied from −0.2 up to 1 \$ L^{-1}, and the P_{BE} was calculated. The concentration of EtOH was 15 wt %. The results were compared with the average prices of hydrogen produced by electrolysis (7.8 \$ $kg_{H_2}^{-1}$), SMR (1.3 \$ $kg_{H_2}^{-1}$), and SMR with carbon capture (SMR + CC, 1.9 \$ $kg_{H_2}^{-1}$) in Germany between 2020 and 2022. The prices of H_2 from the different technologies are taken from George et al.,[82] who investigated thoroughly the impact of state-induced price components on the levelized costs of green, blue, and gray hydrogen in Germany up to 2050. The average electricity price for large industrial consumers in the German market varied in the range of 73.5−78.7 \$ MWh^{-1}.[82] The H_2 selling prices that are used from their study are the ones where no excise tax and price for CO_2 emissions for SMR and SMR + CC are considered. The results are depicted in Figure 13.

The lowest price of EtOH, which is −0.2 \$ L^{-1}, generates the lowest P_{BE} of 2.2 and 0 \$ $kg_{H_2}^{-1}$ for 10 and 50 t h^{-1}, respectively. The base case was 0.56 \$ L^{-1}, accounting for 9.0 \$ $kg_{H_2}^{-1}$ at 10 t h^{-1} and 6.8 \$ $kg_{H_2}^{-1}$ at 50 t h^{-1}. To compete with electrolysis, prices lower than 0.4 \$ L^{-1} are required for the SCWG of 10 t h^{-1}, whereas a price lower than 0.6 \$ L^{-1} is needed for 50 t h^{-1}. Likewise, 50 t h^{-1} can generate hydrogen at the same price as SMR + CC when the feedstock price equals 0.01 \$ L^{-1}. However, negative feedstock prices are needed to reach the value of SMR (i.e., lower than −0.06 \$ L^{-1}). For 10 t h^{-1}, the lowest EtOH price is insufficient to compete with the price of hydrogen from SMR + CC. Therefore, for this technology to be

https://doi.org/10.1021/acs.iecr.4c01486
Ind. Eng. Chem. Res. 2024, 63, 16683−16700

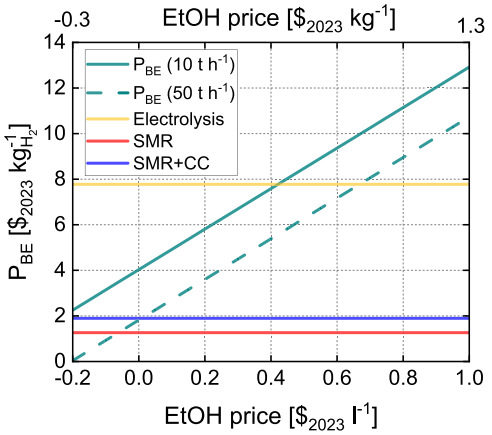

Figure 13. Break-even price of hydrogen as a function of the purchasing price of EtOH, for SCWG of 15 wt % EtOH with 10 and 50 t h^{-1} feed flow rate. Prices of hydrogen from different production technologies are added from literature and are related to the average prices in Germany in the years 2020−2022.[82]

competitive with the others, given that the capacity is in the range of 10−50 t h^{-1}, the price of the raw material must be reduced considerably. Fortunately, biomass offers this possibility.

Alternative waste biomass resources that can be applied in SCWG include microalgae, glycerol, sewage sludge, phenol, sugar cane bagasse, and palm oil mill effluent.[12,83,84] If crude glycerol is used, for example, with a unit cost of 0.21 \$ kg^{-1},[81] this process will produce H_2 with a P_{BE} in the range 3.2−5.4 \$ $kg_{H_2}^{-1}$, from 50 to 10 t h^{-1}, respectively. Due to its excessive production compared to its demand, its price may fall further.[77,81] According to Thilakaratne et al.,[85] algae costs can vary from 0.35 to 7.32 \$ kg^{-1}, depending on their geographic location, strain's properties, extraction and cultivation methods. If algae were used, a minimum price in the range of 4.0−6.2 \$ $kg_{H_2}^{-1}$ (for 50 and 10 t h^{-1}, respectively) would be possible. However, this technology can become extremely expensive if the highest unit price is considered. In the case of sewage sludge, there is a revenue associated with its collection and treatment. Gasafi et al.[75] used a revenue of around 0.26 \$ $kg_{dry\ matter}^{-1}$. By using this value as a negative feedstock price, the P_{BE} price falls in the aforementioned range of 0−2.2 \$ $kg_{H_2}^{-1}$ (for a feed flow rate in the specified range of 10−50 t h^{-1}). Even higher revenues for sewage sludge can be used, e.g., 0.481 \$ $kg_{dry\ matter}^{-1}$.[71] Consequently, with appropriate incentives, sewage sludge gasification can be as competitive as steam reforming of natural gas.

The use of real biomass feedstocks is associated with certain technical challenges. Most of them contain inorganic salt building elements, which can lead to metals corrosion, clogging,[8,13,81,86] and even deactivate the SMR catalyst.[87] The separation of salts can be achieved by specially designed arrangements of the SCWG reactor[8,86,88] or by a continuous treatment upstream of the SCWG reactor.[25] In particular, sewage sludge requires a feed conditioning process before gasification.[25] Gasafi et al.[75] estimated that the feeding equipment accounts for roughly 3.5% of the equipment purchasing costs. A decisive element in the design of this technology is the eventual presence of sulfur in the biomass, as the sulfur-containing species, especially the H_2S, can poison the SMR and WGS catalysts.[51,89,90] The adsorption of H_2S can be done in an adsorber filled with a ZnO-based adsorbent that can work under high temperatures (400 °C).[12,87] These technical modifications lead to additional equipment purchasing costs that, in turn, increase production costs. In some cases, they even increase the $OPEX_{dir}$, e.g., for the case of H_2S adsorption. However, as the sensitivity analysis showed, a decrease in feedstock costs is likely to outweigh and should most probably prevail over the additional investment costs, leading to a lower P_{BE}. Similarly, the increase in electricity and adsorbents demand is expected to be less significant than the decrease in feedstock costs.

CONCLUSIONS

A new kinetic model based on Xu and Froment's model was developed for the steam reforming of the product gas from EtOH SCWG, a reforming process that has yet to be studied extensively. The resulting model simulated the experimental data adequately, predicting the influence of temperature and GHSV, while moderate overestimations were found for the pressure effect. This model is not universal and should only be implemented in a similar reaction system to the one presented in this study, i.e., very low partial pressure of methane and with the consideration of possible internal diffusion control limitations under atmospheric pressure and high temperature.

The techno-economic analysis addressed a hydrogen production process by gasifying biomass model compounds with supercritical water and subsequent steam reforming of the gasification product. As already used in the experimental work, ethanol was used as a biomass model compound and its use accounts for a baseline case. The steam reformer uses the entire amount of water from the feedstock without intermediate separation. The energy needs of the steam reformer are met by the oxyfuel combustion of the residual gas and a small part of the produced hydrogen. Oxyfuel combustion is implemented using oxygen separated from air, so that carbon dioxide is produced at sufficiently high purity to be sold. In addition to hydrogen and carbon dioxide, high and low pressure steam is produced, which can serve as a sales product in adjacent chemical plants.

The economic analysis of the proposed process was based on the break-even price of the hydrogen produced. It was found that the price of hydrogen can be reduced significantly with increasing ethanol concentration, from 40.1 \$ $kg_{H_2}^{-1}$ for 8 wt % EtOH to 17.9 \$ $kg_{H_2}^{-1}$ for 20 wt % EtOH, at 1 t h^{-1} feed flow rate. In practice, however, technical constraints such as gasification efficiency do not allow very high concentrations of organics. Therefore, the concentration proposed for this chemical process is 15 wt %. A further reduction in the hydrogen break-even price was achieved by increasing the feed flow rate. A sharp reduction was possible up to 50 t h^{-1}, with the hydrogen price falling to 6.8 \$ $kg_{H_2}^{-1}$, but further capacity increases did not lead to significant differences. The latter results are consistent with the constraints imposed by biomass feedstock availability, making the upper feed rate limit 50 t h^{-1}.

A sensitivity analysis was performed and found that the most significant contributor to the break-even price of H_2 was the price of EtOH. The current price of ethanol does not accurately represent other waste biomass feedstocks with high water content; hence, other values were considered. The value of crude glycerol enabled the production of H_2 with a minimum break-even price of 3.2 \$ $kg_{H_2}^{-1}$, at 50 t h^{-1} and 15 wt % EtOH, approximately 2.4 times lower than the current price of

https://doi.org/10.1021/acs.iecr.4c01486
Ind. Eng. Chem. Res. 2024, 63, 16683−16700

hydrogen produced by electrolysis in Germany. Using sewage sludge may result in the highest possible profitability due to the revenues associated with its treatment. A feedstock price in the range of −0.26 to 0 \$ kg^{-1} leads to a break-even price between 0 and 1.8 \$ $kg_{H_2}^{-1}$, which falls to the same current price range with the conventional technologies, i.e., of natural gas steam reforming and steam reforming with carbon capture. These findings, however, rule out the specific technical modifications that must be integrated when dealing with actual waste biomass, e.g., salt separation, which are expected to increase the final break-even price of H_2 somewhat.

Future research should assess this process when real waste biomass is implemented, thus providing a more accurate estimate of the hydrogen break-even price. In addition, different arrangements between energy-intensive units and heat exchangers can be investigated and combined with an exergy analysis to make the overall process depend as slightly on the external energy supply as possible.

■ ASSOCIATED CONTENT

Supporting Information

The Supporting Information is available free of charge at https://pubs.acs.org/doi/10.1021/acs.iecr.4c01486.

Additional experimental data, materials, methods, and additional results data, including tables, and figures (PDF)

■ AUTHOR INFORMATION

Corresponding Author

Athanasios A. Vadarlis − *Karlsruhe Institute of Technology (KIT), Institute of Catalysis Research and Technology (IKFT), 76344 Eggenstein-Leopoldshafen, Germany;* orcid.org/0009-0000-3209-7896; Phone: +49 721 608 23388; Email: athanasios.vadarlis@kit.edu

Authors

Bruno Lacerda de Oliveira Campos − *Karlsruhe Institute of Technology (KIT), Institute of Catalysis Research and Technology (IKFT), 76344 Eggenstein-Leopoldshafen, Germany;* orcid.org/0000-0002-1820-5173

Angeliki A. Lemonidou − *Department of Chemical Engineering, Aristotle University of Thessaloniki (AUTH), GR-54124 Thessaloniki, Greece; Chemical Process Engineering Research Institute (CERTH/CPERI), Thessaloniki 57001, Greece;* orcid.org/0000-0001-8376-0678

Nikolaos Boukis − *Karlsruhe Institute of Technology (KIT), Institute of Catalysis Research and Technology (IKFT), 76344 Eggenstein-Leopoldshafen, Germany*

Jörg Sauer − *Karlsruhe Institute of Technology (KIT), Institute of Catalysis Research and Technology (IKFT), 76344 Eggenstein-Leopoldshafen, Germany;* orcid.org/0000-0003-3133-4110

Complete contact information is available at: https://pubs.acs.org/10.1021/acs.iecr.4c01486

Author Contributions

Conceptualization, A.A.V., B.L.d.O.C., N.B., and J.S.; methodology, A.A.V. and B.L.d.O.C.; validation, A.A.V., B.L.d.O.C., A.A.L., N.B., and J.S.; investigation, A.A.V., B.L.d.O.C., and A.A.L.; resources, N.B. and J.S.; writing/original draft preparation, A.A.V., B.L.d.O.C.; writing/review and editing, A.A.L., N.B., and J.S.; visualization, A.A.V., B.L.d.O.C., and J.S.; supervision, A.A.L., and J.S.; All authors have given approval to the final version of the manuscript.

Funding

This work was financed by the research project: Helmholtz European Partnership for Technological Advancement (HEPTA) (grant agreement no. PIE-0016).

Notes

The authors declare no competing financial interest.

■ ACKNOWLEDGMENTS

This work was supported by the research project: Helmholtz European Partnership for Technological Advancement (HEPTA) (grant agreement no. PIE-0016).

■ ABBREVIATIONS

BPR, back pressure regulator; EtOH, ethanol; GHSV, gas hourly space velocity; NPC, net production costs; $OPEX_{dir}$, direct operating expenditures; $OPEX_{ind}$, indirect operating expenditures; P_{BE}, break-even price of hydrogen; PFR, plug flow reactor; PSA, pressure swing adsorption; RDS, rate determining step; SCWG, supercritical water gasification; SER, steam ethane reforming; SMR, steam methane reforming; SR, steam reforming; WGS, water gas shift; WHSV, weight hourly space velocity

■ REFERENCES

(1) Schöb, T.; Kullmann, F.; Linßen, J.; Stolten, D. The Role of Hydrofgen for a Greenhouse Gas-Neutral Germany by 2045. *Int. J. Hydrogen Energy* **2023**, *48* (99), 39124−39137.

(2) Shahbaz, M.; Al-Ansari, T.; Aslam, M.; Khan, Z.; Inayat, A.; Athar, M.; Naqvi, S. R.; Ahmed, M. A.; McKay, G. A State of the Art Review on Biomass Processing and Conversion Technologies to Produce Hydrogen and Its Recovery via Membrane Separation. *Int. J. Hydrogen Energy* **2020**, *45* (30), 15166−15195.

(3) Lee, C. S.; Conradie, A. V.; Lester, E. Review of Supercritical Water Gasification with Lignocellulosic Real Biomass as the Feedstocks: Process Parameters, Biomass Composition, Catalyst Development, Reactor Design and Its Challenges. *Chem. Eng. J.* **2021**, *415*, 128837.

(4) Ferreira-Pinto, L.; Silva Parizi, M. P.; Carvalho de Araújo, P. C.; Zanette, A. F.; Cardozo-Filho, L. Experimental Basic Factors in the Production of H2 via Supercritical Water Gasification. *Int. J. Hydrogen Energy* **2019**, *44* (47), 25365−25383.

(5) Su, H.; Yan, M.; Wang, S. Recent Advances in Supercritical Water Gasification of Biowaste Catalyzed by Transition Metal-Based Catalysts for Hydrogen Production. *Renew. Sustain. Energy Rev.* **2022**, *154*, 111831.

(6) Brito, J.; Pinto, F.; Ferreira, A.; Soria, M. A.; Madeira, L. M. Steam Reforming of Biomass Gasification Gas for Hydrogen Production: From Thermodynamic Analysis to Experimental Validation. *Fuel Process. Technol.* **2023**, *250*, 107859.

(7) Rodriguez Correa, C.; Kruse, A. Supercritical Water Gasification of Biomass for Hydrogen Production - Review. *J. Supercrit. Fluids* **2018**, *133*, 573−590.

(8) Dutzi, J.; Boukis, N.; Sauer, J. Process Effluent Recycling in the Supercritical Water Gasification of Dry Biomass. *Processes* **2023**, *11* (3), 797.

(9) Matsumura, Y.; Minowa, T.; Potic, B.; Kersten, S. R. A.; Prins, W.; Van Swaaij, W. P. M.; Van De Beld, B.; Elliott, D. C.; Neuenschwander, G. G.; Kruse, A.; Antal, M. J. Biomass Gasification in Near- and Super-Critical Water: Status and Prospects. *Biomass Bioenergy* **2005**, *29* (4), 269−292.

(10) Modell, M. Gasification and Liquefaction of Forest Products in Supercritical Water. In *Fundamentals of Thermochemical Biomass*

Conversion; Overend, R. P., Milne, T. A., Mudge, L. K., Eds.; Springer Netherlands: Dordrecht, 1985; pp 95−119.
(11) Vadarlis, A. A.; Angeli, S. D.; Lemonidou, A. A.; Boukis, N.; Sauer, J. Catalytic Biomass Gasification in Supercritical Water and Product Gas Upgrading. *ChemBioEng Rev.* **2023**, *10* (4), 370−398.
(12) Ruya, P. M.; Lim, S. S.; Purwadi, R.; Zunita, M. Sustainable Hydrogen Production from Oil Palm Derived Wastes through Autothermal Operation of Supercritical Water Gasification System. *Energy* **2020**, *208*, 118280.
(13) Boukis, N.; Stoll, I. K. Gasification of Biomass in Supercritical Water, Challenges for the Process Design-Lessons Learned from the Operation Experience of the First Dedicated Pilot Plant. *Processes* **2021**, *9* (3), 455.
(14) Angeli, S. D.; Monteleone, G.; Giaconia, A.; Lemonidou, A. A. State-of-the-Art Catalysts for CH4 Steam Reforming at Low Temperature. *Int. J. Hydrogen Energy* **2014**, *39* (5), 1979−1997.
(15) Chen, Y.; Yi, L.; Li, S.; Yin, J.; Jin, H. Catalytic Gasification of Sewage Sludge in near and Supercritical Water with Different Catalysts. *Chem. Eng. J.* **2020**, *388*, 124292.
(16) Mohanty, U. S.; Ali, M.; Azhar, M. R.; Al-Yaseri, A.; Keshavarz, A.; Iglauer, S. Current Advances in Syngas (CO + H2) Production through Bi-Reforming of Methane Using Various Catalysts: A Review. *Int. J. Hydrogen Energy* **2021**, *46* (65), 32809−32845.
(17) Pinaeva, L. G.; Noskov, A. S. Modern Level of Catalysts and Technologies for the Conversion of Natural Gas into Syngas. *Ind. Catal.* **2022**, *14* (1), 66−85.
(18) Borowiecki, T. Nickel Catalysts for Steam Reforming of Hydrocarbons; Size of Crystallites and Resistance to Coking. *Appl. Catal.* **1982**, *4* (3), 223−231.
(19) Fowles, M.; Carlsson, M. Steam Reforming of Hydrocarbons for Synthesis Gas Production. *Top. Catal.* **2021**, *64* (17−20), 856−875.
(20) Rostrup-Nielsen, J. R. Activity of Nickel Catalysts for Steam Reforming of Hydrocarbons. *J. Catal.* **1973**, *31*, 173−199.
(21) Rostrup-Nielsen, J. R.; Sehested, J.; Nørskov, J. K. Hydrogen and Synthesis Gas by Steam- and C02 Reforming. *Adv. Catal.* **2002**, *47*, 65−139.
(22) Avetisov, A. K.; Rostrup-Nielsen, J. R.; Kuchaev, V. L.; Bak Hansen, J. H.; Zyskin, A. G.; Shapatina, E. N. Steady-State Kinetics and Mechanism of Methane Reforming with Steam and Carbon Dioxide over Ni Catalyst. *J. Mol. Catal. A: Chem.* **2010**, *315* (2), 155−162.
(23) Hantoko, D.; Su, H.; Yan, M.; Kanchanatip, E.; Susanto, H.; Wang, G.; Zhang, S.; Xu, Z. Thermodynamic Study on the Integrated Supercritical Water Gasification with Reforming Process for Hydrogen Production: Effects of Operating Parameters. *Int. J. Hydrogen Energy* **2018**, *43* (37), 17620−17632.
(24) Campanario, F. J.; Gutiérrez Ortiz, F. J. Techno-Economic Assessment of Bio-Oil Aqueous Phase-to-Liquids via Fischer−Tropsch Synthesis and Based on Supercritical Water Reforming. *Energy Convers. Manag.* **2017**, *154*, 591−602.
(25) Kumar, M.; Oyedun, A. O.; Kumar, A. A Comparative Analysis of Hydrogen Production from the Thermochemical Conversion of Algal Biomass. *Int. J. Hydrogen Energy* **2019**, *44* (21), 10384−10397.
(26) Saim, S.; Subramaniam, B. Isomerization of 1-Hexene over Pt/γ-Al2O3 Catalyst: Reaction Mixture Density and Temperature Effects on Catalyst Effectiveness Factor, Coke Laydown, and Catalyst Micromeritics. *J. Catal.* **1991**, *131* (2), 445−456.
(27) Baptist-Nguyen, S.; Subramaniam, B. Coking and Activity of Porous Catalysts in Supercritical Reaction Media. *AIChE J.* **1992**, *38* (7), 1027−1037.
(28) Subramaniam, B.; McCoy, B. J. Catalyst Activity Maintenance or Decay: A Model for Formation and Desorption of Coke. *Ind. Eng. Chem. Res.* **1994**, *33* (3), 504−508.
(29) Boukis, N.; Vadarlis, A. A.; Sauer, J. Process for Producing Hydrogen and Carbon Dioxide from Organic Substances. EP 4166499 A2, 2023.
(30) Vadarlis, A. A.; Neukum, D.; Lemonidou, A. A.; Boukis, N.; Sauer, J. Direct Steam Reforming of the Product Gas from Ethanol Gasification with Supercritical Water. *Int. J. Hydrogen Energy* **2024**, *49*, 992−1008.
(31) Lagioia, G.; Spinelli, M. P.; Amicarelli, V. Blue and Green Hydrogen Energy to Meet European Union Decarbonisation Objectives. An Overview of Perspectives and the Current State of Affairs. *Int. J. Hydrogen Energy* **2023**, *48*, 1304−1322.
(32) Cardinale, R. From Natural Gas to Green Hydrogen: Developing and Repurposing Transnational Energy Infrastructure Connecting North Africa to Europe. *Energy Pol.* **2023**, *181*, 113623.
(33) Zhou, Y.; Searle, S. Cost of renewable hydrogen produced onsite at hydrogen refueling stations in Europe; The International Council on Clean Transportation: Washington, DC, 2022. https://theicct.org/publication/fuels-eu-onsite-hydro-cost-feb22/ (accessed Aug 12, 2024).
(34) Clerici, A.; Furfari, S. The present and future green hydrogen production cost. https://www.science-climat-energie.be/2021/07/16/the-present-and-future-green-hydrogen-production-cost/ (accessed Aug 09, 2024).
(35) Gong, M.; Zhu, W.; Xu, Z. R.; Zhang, H. W.; Yang, H. P. Influence of Sludge Properties on the Direct Gasification of Dewatered Sewage Sludge in Supercritical Water. *Renew. Energy* **2014**, *66*, 605−611.
(36) Xue, X.; Chen, D.; Song, X.; Dai, X. Hydrothermal and Pyrolysis Treatment for Sewage Sludge: Choice from Product and from Energy Benefit. *Phys. Procedia* **2015**, *66*, 301−304.
(37) Migliaccio, R.; Brachi, P.; Montagnaro, F.; Papa, S.; Tavano, A.; Montesarchio, P.; Ruoppolo, G.; Urciuolo, M. Sewage Sludge Gasification in a Fluidized Bed: Experimental Investigation and Modeling. *Ind. Eng. Chem. Res.* **2021**, *60* (13), 5034−5047.
(38) Gao, N.; Kamran, K.; Quan, C.; Williams, P. T. Thermochemical Conversion of Sewage Sludge: A Critical Review. *Prog. Energy Combust. Sci.* **2020**, *79*, 100843.
(39) Hantoko, D.; Antoni; Kanchanatip, E.; Yan, M.; Weng, Z.; Gao, Z.; Zhong, Y. Assessment of Sewage Sludge Gasification in Supercritical Water for H2-Rich Syngas Production. *Process Saf. Environ. Prot.* **2019**, *131*, 63−72.
(40) Elsayed, S.; Boukis, N.; Patzelt, D.; Hindersin, S.; Kerner, M.; Sauer, J. Gasification of Microalgae Using Supercritical Water and the Potential of Effluent Recycling. *Chem. Eng. Technol.* **2016**, *39* (2), 335−342.
(41) Xu, J.; Froment, G. F. Methane Steam Reforming, Methanation and Water-Gas Shift: I. Intrinsic Kinetics. *AIChE J.* **1989**, *35* (1), 88−96.
(42) Jakobsen, J. G.; Jørgensen, T. L.; Chorkendorff, I.; Sehested, J. Steam and CO2 Reforming of Methane over a Ru/ZrO2 Catalyst. *Appl. Catal., A* **2010**, *377* (1−2), 158−166.
(43) Obradović, A.; Likozar, B.; Levec, J. Steam Methane Reforming over Ni-Based Pellet-Type and Pt/Ni/Al2O3 Structured Plate-Type Catalyst: Intrinsic Kinetics Study. *Ind. Eng. Chem. Res.* **2013**, *52* (38), 13597−13606.
(44) Wei, J.; Iglesia, E. Mechanism and Site Requirements for Activation and Chemical Conversion of Methane on Supported Pt Clusters and Turnover Rate Comparisons among Noble Metals. *J. Phys. Chem. B* **2004**, *108* (13), 4094−4103.
(45) Wójcik, M.; Szabłowski, Ł.; Dybiński, O. Comparison of Mathematical Models of Steam Methane Reforming Process for the Needs of Fuel Cells. *Int. J. Hydrogen Energy* **2024**, *52*, 965−982.
(46) Goos, E.; Burcat, A.; Ruscic, B. Extended third millennium ideal gas and condensed phase thermochemical database for combustion with updates from active thermochemical tables. http://garfield.chem.elte.hu/Burcat/THERM.DAT (accessed Jan 26, 2024).
(47) Peloquin, J.-F.; Francoeur, D.; Leclerc, W.; Mehanovic, D.; Dufault, J.-F.; Camus, P.; Castellanos-Beltran, I. J.; Braidy, N.; Fréchette, L. G.; Picard, M. Electrified Steam Methane Reforming Microreactor. *Int. J. Hydrogen Energy* **2024**, *49*, 907−915.
(48) Meerman, J. C.; Hamborg, E. S.; van Keulen, T.; Ramírez, A.; Turkenburg, W. C.; Faaij, A. P. C. Techno-Economic Assessment of CO2 Capture at Steam Methane Reforming Facilities Using Commercially Available Technology. *Int. J. Greenh. Gas Control* **2012**, *9*, 160−171.

https://doi.org/10.1021/acs.iecr.4c01486
Ind. Eng. Chem. Res. 2024, 63, 16683−16700

(49) Yang, J.; Han, S.; Cho, C.; Lee, C. H.; Lee, H. Bulk Separation of Hydrogen Mixtures by a One-Column PSA Process. *Sep. Technol.* **1995**, *5* (4), 239−249.
(50) Sircar, S.; Rao, M. B.; Golden, T. C. Fractionation of Air by Zeolites. In *Studies in Surface Science and Catalysis*; Dabrowski, A., Ed.; Elsevier Science B. V.: Lublin, Poland, 1999; Vol. *120*, pp 395−423.
(51) Chattanathan, S. A.; Adhikari, S.; McVey, M.; Fasina, O. Hydrogen Production from Biogas Reforming and the Effect of H2S on CH4 Conversion. *Int. J. Hydrogen Energy* **2014**, *39* (35), 19905−19911.
(52) Dutzi, J.; Vadarlis, A. A.; Boukis, N.; Sauer, J. Comparison of Experimental Results with Thermodynamic Equilibrium Simulations of Supercritical Water Gasification of Concentrated Ethanol Solutions with Focus on Water Splitting. *Ind. Eng. Chem. Res.* **2023**, *62* (32), 12501−12512.
(53) Towler, G. P.; Sinnott, R. K. *Chemical Engineering Design: Principles, Practice, and Economics of Plant and Process Design*; Butterworth-Heinemann, 2013.
(54) Bongartz, D.; Burre, J.; Mitsos, A. Production of Oxymethylene Dimethyl Ethers from Hydrogen and Carbon Dioxide - Part I: Modeling and Analysis for OME1. *Ind. Eng. Chem. Res.* **2019**, *58* (12), 4881−4889.
(55) Lacerda de Oliveira Campos, B.; John, K.; Beeskow, P.; Herrera Delgado, K.; Pitter, S.; Dahmen, N.; Sauer, J. A Detailed Process and Techno-Economic Analysis of Methanol Synthesis from H2 and CO2 with Intermediate Condensation Steps. *Processes* **2022**, *10* (8), 1535.
(56) Peters, M. S.; Timmerhaus, K. D.; West, R. E. *Plant Design and Economics for Chemical Engineers*, 5th ed.; Glandt, E. D.; Klein, M. T.; Edgar, T. F., Eds.; McGraw-Hill, 1959; Vol. *5*.
(57) Chemical Engineering Essentials for the CPI Professional-November 2021-48. New York, September 2023. www.chemengonline.com (accessed Dec 12, 2023).
(58) Albrecht, F. G.; König, D. H.; Baucks, N.; Dietrich, R. U. A Standardized Methodology for the Techno-Economic Evaluation of Alternative Fuels - A Case Study. *Fuel* **2017**, *194*, 511−526.
(59) Lee, S.; Kim, H. S.; Park, J.; Kang, B. M.; Cho, C.-H.; Lim, H.; Won, W. Scenario-Based Techno-Economic Analysis of Steam Methane Reforming Process for Hydrogen Production. *Appl. Sci.* **2021**, *11* (13), 6021.
(60) Ethanol price. https://www.finanzen.net/rohstoffe/ethanolpreis (accessed Oct 10, 2023).
(61) Yan, Y.; Manovic, V.; Anthony, E. J.; Clough, P. T. Techno-Economic Analysis of Low-Carbon Hydrogen Production by Sorption Enhanced Steam Methane Reforming (SE-SMR) Processes. *Energy Convers. Manag.* **2020**, *226*, 113530.
(62) Granjo, J. F. O.; Oliveira, N. M. C. Process Simulation and Techno-Economic Analysis of the Production of Sodium Methoxide. *Ind. Eng. Chem. Res.* **2016**, *55* (1), 156−167.
(63) Kim, T. W.; Park, J. C.; Lim, T. H.; Jung, H.; Chun, D. H.; Lee, H. T.; Hong, S.; Yang, J. The Kinetics of Steam Methane Reforming over a Ni/γ-Al2O3 Catalyst for the Development of Small Stationary Reformers. *Int. J. Hydrogen Energy* **2015**, *40* (13), 4512−4518.
(64) Oliveira, E. L. G.; Grande, C. A.; Rodrigues, A. E. Steam Methane Reforming in a Ni/Al2O3 Catalyst: Kinetics and Diffusional Limitations in Extrudates. *Can. J. Chem. Eng.* **2009**, *87* (6), 945−956.
(65) Mears, D. E. Tests for Transport Limitations in Experimental Catalytic Reactors. *Ind. Eng. Chem. Process Des. Dev.* **1971**, *10* (4), 541−547.
(66) Weisz, P. B.; Prater, C. D. Interpretation of Measurements in Experimental Catalysis. *Adv. Catal.* **1954**, *6* (C), 143−196.
(67) Thiele, E. W. Relation between Catalytic Activity and Size of Particle. *Ind. Eng. Chem.* **1939**, *31* (7), 916−920.
(68) Vannice, M. A. *Kinetics of Catalytic Reactions*; Springer Science + Business Media, Inc, 2005.
(69) Ahmed, S.; Lee, S. H. D.; Ferrandon, M. S. Catalytic Steam Reforming of Biogas - Effects of Feed Composition and Operating Conditions. *Int. J. Hydrogen Energy* **2015**, *40* (2), 1005−1015.
(70) Chen, L.; Qi, Z.; Zhang, S.; Su, J.; Somorjai, G. A. Catalytic Hydrogen Production from Methane: A Review on Recent Progress and Prospect. *Catalysts* **2020**, *10* (8), 858.
(71) *Near-Critical and Supercritical Water and Their Applications for Biorefineries*; Fang, Z., Xu, C., Eds.; Biofuels and Biorefineries: Springer Dordrecht, 2014; Vol. *2*.
(72) Vivanpatarakij, S.; Assabumrungrat, S. Thermodynamic Analysis of Combined Unit of Biomass Gasifier and Tar Steam Reformer for Hydrogen Production and Tar Removal. *Int. J. Hydrogen Energy* **2013**, *38* (10), 3930−3936.
(73) Gao, N.; Wang, X.; Li, A.; Wu, C.; Yin, Z. Hydrogen Production from Catalytic Steam Reforming of Benzene as Tar Model Compound of Biomass Gasification. *Fuel Process. Technol.* **2016**, *148*, 380−387.
(74) Acelas, N. Y.; López, D. P.; Wim Brilman, D. W. F.; Kersten, S. R. A.; Kootstra, A. M. J. Supercritical Water Gasification of Sewage Sludge: Gas Production and Phosphorus Recovery. *Bioresour. Technol.* **2014**, *174*, 167−175.
(75) Gasafi, E.; Reinecke, M. Y.; Kruse, A.; Schebek, L. Economic Analysis of Sewage Sludge Gasification in Supercritical Water for Hydrogen Production. *Biomass Bioenergy* **2008**, *32* (12), 1085−1096.
(76) Einwohnerzahl der größten Städte in Deutschland am 31. Dezember 2022, Statistisches Bundesamt. https://de.statista.com/statistik/daten/studie/1353/umfrage/einwohnerzahlen-der-grossstaedte-deutschlands/ (accessed Jan 22, 2024).
(77) Galera, S.; Gutiérrez Ortiz, F. Techno-Economic Assessment of Hydrogen and Power Production from Supercritical Water Reforming of Glycerol. *Fuel* **2015**, *144*, 307−316.
(78) Chakinala, A. G.; Brilman, D. W. F.; Van Swaaij, W. P. M.; Kersten, S. R. A. Catalytic and Non-Catalytic Supercritical Water Gasification of Microalgae and Glycerol. *Ind. Eng. Chem. Res.* **2010**, *49* (3), 1113−1122.
(79) Gutiérrez Ortiz, F.; Ollero, P.; Serrera, A.; Galera, S. Process Integration and Exergy Analysis of the Autothermal Reforming of Glycerol Using Supercritical Water. *Energy* **2012**, *42* (1), 192−203.
(80) Gutiérrez Ortiz, F.; Ollero, P.; Serrera, A.; Galera, S. An Energy and Exergy Analysis of the Supercritical Water Reforming of Glycerol for Power Production. *Int. J. Hydrogen Energy* **2012**, *37* (1), 209−226.
(81) Attarbachi, T.; Kingsley, M. D.; Spallina, V. New Trends on Crude Glycerol Purification: A Review. *Fuel* **2023**, *340*, 127485.
(82) George, J. F.; Müller, V. P.; Winkler, J.; Ragwitz, M. Is Blue Hydrogen a Bridging Technology? - The Limits of a CO2 Price and the Role of State-Induced Price Components for Green Hydrogen Production in Germany. *Energy Pol.* **2022**, *167*, 113072.
(83) Fiori, L.; Valbusa, M.; Castello, D. Supercritical Water Gasification of Biomass for H2 Production: Process Design. *Bioresour. Technol.* **2012**, *121*, 139−147.
(84) Safari, F.; Tavasoli, A.; Ataei, A. Gasification of Sugarcane Bagasse in Supercritical Water Media for Combined Hydrogen and Power Production: A Novel Approach. *Int. J. Environ. Sci. Technol.* **2016**, *13* (10), 2393−2400.
(85) Thilakaratne, R.; Wright, M. M.; Brown, R. C. A Techno-Economic Analysis of Microalgae Remnant Catalytic Pyrolysis and Upgrading to Fuels. *Fuel* **2014**, *128*, 104−112.
(86) Boukis, N.; Galla, U.; Müller, H.; Dinjus, E. Hydrothermal Gasification of Glycerol on the Pilot Scale. *16th European Biomass Conference & Exhibition*, 2008.
(87) Peng, G.; Ludwig, C.; Vogel, F. Catalytic Supercritical Water Gasification: Interaction of Sulfur with ZnO and the Ruthenium Catalyst. *Appl. Catal., B* **2017**, *202*, 262−268.
(88) Dutzi, J.; Boukis, N.; Sauer, J. Supercritical Water Gasification of Heavy Metal Contaminated Plants with Focus on Separation of Heavy Metal Contaminants. *Biomass Bioenergy* **2024**, *182*, 107059.
(89) Koningen, J.; Sjöström, K. Sulfur-Deactivated Steam Reforming of Gasified Biomass. *Ind. Eng. Chem. Res.* **1998**, *37* (2), 341−346.
(90) Gillan, C.; Fowles, M.; French, S.; Jackson, S. D. Ethane Steam Reforming over a Platinum/Alumina Catalyst: Effect of Sulfur Poisoning. *Ind. Eng. Chem. Res.* **2013**, *52* (37), 13350−13356.

https://doi.org/10.1021/acs.iecr.4c01486
Ind. Eng. Chem. Res. 2024, 63, 16683−16700